

Copyright Warning & Restrictions

The copyright law of the United States (Title 17, United States Code) governs the making of photocopies or other reproductions of copyrighted material.

Under certain conditions specified in the law, libraries and archives are authorized to furnish a photocopy or other reproduction. One of these specified conditions is that the photocopy or reproduction is not to be “used for any purpose other than private study, scholarship, or research.” If a user makes a request for, or later uses, a photocopy or reproduction for purposes in excess of “fair use” that user may be liable for copyright infringement,

This institution reserves the right to refuse to accept a copying order if, in its judgment, fulfillment of the order would involve violation of copyright law.

Please Note: The author retains the copyright while the New Jersey Institute of Technology reserves the right to distribute this thesis or dissertation

Printing note: If you do not wish to print this page, then select “Pages from: first page # to: last page #” on the print dialog screen



The Van Houten library has removed some of the personal information and all signatures from the approval page and biographical sketches of theses and dissertations in order to protect the identity of NJIT graduates and faculty.

ABSTRACT

INSTABILITY OF ELECTRIFIED VISCOUS FILMS

by
Knograt Savettaseranee

We examine the stability of a thin two-dimensional liquid film with a regular electric field applied in a direction parallel to an initially flat bounding fluid interface. We study the distinct physical effects of surface tension, van der Waals and electrically induced forces for a viscous incompressible fluid. The film is assumed to be sufficiently thin, and the surface tension and electrically induced forces are large enough that gravity can be ignored to the leading order. Our target is to analyse the nonlinear stability of the flow. We attain this by deriving and numerically solving a set of nonlinear evolution equations for the local film thickness and for symmetrical interfacial perturbations. We find that the electric field forces enhance the stability of the flow and can remove rupture.

INSTABILITY OF ELECTRIFIED VISCOUS FILMS

by
Knograt Savettaseranee

**A Dissertation
Submitted to the Faculty of
New Jersey Institute of Technology and
Rutgers, The State University of New Jersey – Newark
in Partial Fulfillment of the Requirements for the Degree of
Doctor of Philosophy in Mathematical Sciences**

**Department of Mathematical Sciences
Department of Mathematics and Computer Science, Rutgers-Newark**

May, 2002

Copyright © 2002 by Knograt Savettaseranee
ALL RIGHTS RESERVED

APPROVAL PAGE

INSTABILITY OF ELECTRIFIED VISCOUS FILMS

Knograt Savettaseranee

5/08/02

Dr. Demetrius T. Papageorgiou, Dissertation Advisor
Professor of Mathematical Sciences, NJIT, Newark NJ

Date

5/8/02

Dr. Daljit S. Ahluwalia, Committee Member
Chairperson and Professor of Mathematical Sciences, NJIT, Newark NJ

Date

5/08/02

Dr. Charles Maldarelli, Committee Member
Professor of Chemical Engineering, CCNY, New York, NY

Date

5/8/02

Dr. Peter G. Petropoulos, Committee Member
Associate Professor of Mathematical Sciences, NJIT, Newark NJ

Date

5/8/02

Dr. Lou Kondic, Committee Member
Assistant Professor of Mathematical Sciences, NJIT, Newark NJ

Date

BIOGRAPHICAL SKETCH

Author: Knograt Savettaseranee

Degree: Doctor of Philosophy

Date: May 2002

Date of Birth:

Place of Birth:

Undergraduate and Graduate Education:

- Doctor of Philosophy in Mathematical Sciences,
New Jersey Institute of Technology and Rutgers University, Newark, NJ, 2002
- Master of Science in Applied Mathematics,
New Jersey Institute of Technology, Newark, NJ, 2000
- Master of Science in Mathematics,
Chulalongkorn University, Bangkok, Thailand, 1991
- Bachelor of Science in Mathematics,
Chulalongkorn University, Bangkok, Thailand, 1987

Major: Mathematical Sciences

To Buddhas in nivana, Laung Por Sod, Laung Por Dhamma and Khun Yai Chun
Khonnokyoong

ACKNOWLEDGMENT

I wish to express my gratitude to my Advisor, Dr. Demetrius T. Papageorgiou for his immense contribution, guidance, and patience with me. I also wish to thank the other members of my dissertation committee, Professors Ahluwalia, Maldarelli, Petropoulos and Kondic. I would like to particularly thank Drs. Petropoulos and Tilley who offered me time from their busy schedules during my research. I also wish to thank all my other professors, friends, and fellow students at NJIT during these years of study. Spacial thanks go to my friends Said Kas-Danouche, Urmi Ghosh Dastidar, Hoa K. Tran and Lyudmyla Barannyk.

I would like to extend my grateful thanks to Kasetsart University, Thailand, for providing me of a full scholarship during my stay in NJIT.

Finally, I would like to express my deepest appreciation to my parents, General Ratana and Rewadee Savettaseranee, who gave me the precious gift of life. Adirek Savettaseranee, my brother, is deserving of recognition for inspiring me to pursue a doctoral degree in Mathematical Sciences.

TABLE OF CONTENTS

Chapter	Page
1 INTRODUCTION AND LITERATURE REVIEW	1
2 MATHEMATICAL MODEL	5
2.1 Physical Problem and Governing Equations	5
2.2 Nondimensionalization of the governing equations	8
3 LINEAR STABILITY	13
3.1 Derivation of the Linear Stability Equations	13
3.2 Solution of the Linear Problem and the Dispersion Relation	15
3.3 Asymptotic Results For Small ϵ And Scales For The Nonlinear Theory	22
4 NONLINEAR STABILITY	24
4.1 Derivation Of The Nonlinear Evolution Equations	24
4.2 Linear Stability Analysis of the Evolution Equations	33
5 NUMERICAL SOLUTION OF THE EVOLUTION EQUATIONS	36
5.1 Numerical Solutions	36
5.2 The Case of Zero Electric Field and Similarity Solutions	37
5.3 Non-zero Electric Field	40
6 CONCLUSIONS	52
BIBLIOGRAPHY	53

LIST OF TABLES

Table		Page
5.1	Estimation of scaling exponents for no electric field	40
5.2	Estimation of scaling exponents in the presence of an electric field	42

LIST OF FIGURES

Figure	Page
3.1	The relation between wave number k and growth rates ω with different E_b in equation (3.21) 18
3.2	The relation between wave number k and growth rate ω for different ε in equation (3.21) 18
3.3	The relation between van der Waals forces, surface tension and k_{max} for different V in equation (3.21) 19
3.4	The relation between van der Waals forces, surface tension and k_{cut} for different E_b in equation (3.21) 20
3.5	The relation between van der Waals forces, surface tension and k_{max} for different ε in equation (3.21) 21
3.6	The relation between van der Waals forces, surface tension and k_{cut} for different ε in equation (3.21) 21
4.1	The three regions for the asymptotic solution. 27
4.2	The relation. For (a) wave number k and growth rate ω with different \bar{E}_b . For (b) \bar{E}_b and k_c 35
5.1	The evolution of $H(x, t)$ and $u(x, t)$ for $Re = 1/\pi$, $K = 8$, $W_e = 0$, $W_f = 1.5$. (a) The evolution of $H(x, t)$. (b) The evolution of $u(x, t)$ 39
5.2	No electric field. Evolution of (a) H_{min} , (b) u_{max} and (c) $\max(u_x)$ for $K = 8$, $W_e = 0$, $W_f = 1.5$ 39
5.3	The relation between $\log_{10}H(\pi, t)$ with $u_x(\pi, t)$, $-H_t(\pi, t)$, $H_{xx}(\pi, t)$, $umax(x, t)$, and $\max(H_x(x, t))$ respectively. Computed slopes are given in Table 5.1. 41
5.4	Electric field present. $K = 8$, $W_e = 0.5$, $W_f = 1.5$. (a) Evolution of $H(x, t)$, (b) evolution of $u(x, t)$ 42
5.5	Electric field present. $K = 8$, $W_e = 0.5$, $W_f = 1.5$. (a) Evolution of H_{min} . (b) Evolution of $max(u)$. (c) Evolution of $max(u_x)$ 43
5.6	The relation between $\log_{10}H(\pi, t)$ with $u_x(\pi, t)$, $-H_t(\pi, t)$, $H_{xx}(\pi, t)$, $umax(x, t)$, and $\max(H_x(x, t))$ respectively. Computed slopes are given in Table 5.2. 43
5.7	Evolution of $E(t) = \int_0^{2\pi} (H^2 + u^2)dx$, $K = 8$, $W_f = 1.5$. (a) No electric field, $W_e = 0$. (b) $W_e = 0.5$ 44
5.8	Relatively large electric field, $W_e = 2.0$, showing stabilization. (a) Evolution of $H(x, t)$. (b) Evolution of $u(x, t)$ 45

LIST OF FIGURES
(Continued)

Figure	Page
5.9 Relatively large electric field, $W_e = 2.0$, showing stabilization. $K = 8, W_e = 2, W_f = 1.5$. (a) Evolution of H_{min} . (b) Evolution of $max(u)$. (c) Evolution of $max(u_x)$	46
5.10 Rupture time as a function of W_e for the set of initial conditions (5.3). .	46
5.11 Small amplitude initial conditions $H(x, 0) = 1 + 0.01 \cos(x)$ and $W_e = 1.55$. (a) The evolution of $H(x, t)$. (b) The evolutions $u(x, t)$	48
5.12 Initial conditions $u(x, 0) = 0, H(x, 0) = 1 + 0.01 \cos(x), W_e = 1.55$. Behavior above linear threshold. (a) Evolution of H_{min} . (b) Evolution of $max(u)$. (c) Evolution of $max(u_x)$	49
5.13 Initial conditions $u(x, 0) = 0, H(x, 0) = 1 + 0.01 \cos(x), W_e = 1.45$. (a) The evolution of $H(x, t)$. (b) The evolutions $u(x, t)$	49
5.14 Initial conditions $u(x, 0) = 0, H(x, 0) = 1 + 0.01 \cos(x), W_e = 1.45$. Behavior below linear threshold. (a) Evolution of H_{min} . (b) Evolution of $max(u)$. (c) Evolution of $max(u_x)$	50
5.15 Initial conditions $H(x, 0) = 1 + 0.01 \cos(x), u(x, 0) = 0. K = 8, W_f = 1.5, Re = 1/\pi$. Evolution of H_{min} for increasing values of W_e	50
5.16 Initial conditions $H(x, 0) = 1 + 0.01 \cos(x), u(x, 0) = 0. K = 8, W_f = 1.5, Re = 1/\pi$. Evolution of H_{min} for increasing values of W_e	51

CHAPTER 1

INTRODUCTION AND LITERATURE REVIEW

Macroscopic thin liquid films are important in a variety of applications from biophysics and engineering. One of the important and central phenomena in the dynamics of thin films, is the phenomenon of rupture. Many physical processes involve rupture phenomena and more specifically that of free liquid films. For example, instability and rupture of such films can be found in colloid and bicolloid systems and particular applications involve the rupture of soap films, coalescence of emulsions, fusion of lipid bilayers or biological membranes, to mention a few (see for example Prevost and Gallez [14] and references therein). In engineering applications, thin films are explored in heat and mass transfer process to limit fluxes and to protect surfaces in extreme operating conditions..

A liquid layer on a plain solid boundary is unstable when the layer is ultrathin ($100 - 1000 \text{ \AA}$). The instability occurs due to long-range van der Waals molecular forces which can cause rupture of the layer. Deryagin [2] first recognized that an excess pressure can be found in a thin liquid layer compared with the pressure in the bulk phase - he termed this excess pressure the "disjoining pressure". A negative disjoining pressure is found in films with higher pressure than that of the bulk phases as when van der Waals forces between bodies whose characteristic dimensions are large compared to interatomic distance; in this case thinning occurs leading to rupture. In the presence of electric double-layer potentials, a stabilizing competition is set up due to the positive disjoining pressure of the new effect. This can then lead to what are called black films as described by Overbeek [13].

Vrij [20] examined the problem of finding the thickness at which a nondraining film became unstable because of van der Waals forces. A static stability analysis is used to calculate a marginally stable thickness at which small disturbance first start

to grow. Ruckenstein and Jain [16] consider a more general stability theory for a film on a horizontal plate. The theory was based on the Navier-Stokes equations modified by the van der Waals forces. They find that the most unstable wave has a wavelength which is large compared to the film thickness. The linear stability of radially bounded thinning free films for which the base state is time dependent (and calculated by lubrication theory) was investigated by Gumerman and Homsy [7]. The nonlinear problem of a liquid film on a solid substrate was addressed by Williams and Davis [22], who used long wave asymptotics to derive a nonlinear partial differential equation capable of describing large amplitude disturbances (the disturbances scale with the film thickness but are long compared to it). The evolution equation retains the effects of surface tension, viscous and van der Waals forces. The equation was solved numerically by Burelbach, Bankoff and Davis [1], who examined the structures near rupture. Much more accurate numerical solutions capable of resolving the singularity structure, have been carried out by Zhang and Lister [24], who also propose similarity solutions for the singularity. The stability of such similarity solutions is considered by Witelski and Bernoff [23].

Work on the linear stability of a free film has been carried out by Ruckenstein and Jain [16]. Prevost and Gallez [15], [14] attempted to derive a nonlinear evolution equation by using long wave theories and managed to do so for relatively large values of surface viscosity; this leads to a single nonlinear partial differential equation for the interface and the effects of surface tension and van der Waals forces are included. Sharma and Ruckenstein [17] studied this case as well and got a valid nonlinear evolution equation for the interface shape. A more general situation is described by the work of Erneux and Davis [4], who derive a coupled set of evolution equations starting from the Navier-Stokes equations. Numerical solutions of these equations are considered by Ida and Miksis in a series of articles [8], [9], [10]. A comprehensive review of the subject of the stability of thin films can be found in Oron, Davis, and

Bankoff[12]. A recent numerical study of the Erneux and Davis evolution equations has been carried out by Vaynblat, Lister and Witelki [19], who use adaptive grids to integrate accurately to times very close to the singularity and are thus able to resolve the structure in a definitive way. It is found that at rupture the main balances are between inertia, viscosity and van der Waals forces, with surface tension forces negligible. This leads to similarity solutions of the first kind as opposed to those of the second kind proposed by Ida and Miksis. Our work is consistent with the findings of [19].

When electric fields are present there are additional physical effects including body forces due to currents in conducting fluids, and Maxwell stresses at free interfaces. Melcher and Schwarz [11] examined the effect of an electric field on the linear stability of a sharp interface separating two non-conducting dielectric fluids of infinite extent. A constant electric field was applied in the plane of the undisturbed interface and they investigated the linear stability of viscous and inviscid fluid in the absence of van der Waals forces. El-Sayed [3] considered the linear stability of an electrified fluid sheet when aerodynamic effects in the surrounding medium are important and found that the field stabilizes the flow. Wendel, Gallez and Bisch [21], consider the stability of a dielectric film in the presence of double layer potentials. The potential and charge distributions in the film are taken as given, and two cases are studied: a linear potential drop across the film and no charge on the interfaces, and, finite surface charge on the interfaces and zero potential drop across the film. A linear stability analysis is carried out in the presence of van der Waals forces, which shows that the surface charge induces oppositely charged double layers that enhance the van der Waals instability.

In the case of perfectly conducting viscous fluids, a normal electric field can destabilize the interface. Gonzalez and Castellanos [6], studied the nonlinear stability of perfectly conducting film flow down an inclined plane, and derived a nonlinear

evolution equation which includes a Hilbert transform type term due to the electric field. A weakly nonlinear version of this equation provides a modification of the Kuramoto-Sivashinsky equation with the electric field acting to add or remove active modes to the system. Qualitative features are given, but a careful numerical study has not been carried out.

Tilley, Petropoulos and Papageorgiou [18] investigated the stability of a thin two dimensional liquid film when a uniform electric field was applied in a direction parallel to the initially bounding interface and examined the distinct physical effect of surface tension and electrically induced force for an inviscid, incompressible non-conducting fluid. They analyzed the nonlinear stability of the flow by deriving a set of evolution equations for the local film thickness and local horizontal velocity. Periodic traveling waves were examined and their behavior was studied as the electric field was increased. A modulational instability of the wave trains was also found in both the absence and presence of an electric field, and it was shown that very low level but long perturbations can lead to film rupture. They carried out extensive simulations of the initial value problem that showed that the presence of the electric field caused a nonlinear stabilization.

In the present work, we derive a system of nonlinear evolution equations that govern the stability of free films in the presence of a horizontal electric field. The electric field effects appear as a non-local term proportional to the Hilbert transform of the leading order interfacial curvature. We are able to study the competing effects of inertia, van der Waals forces, surface tension and electric fields. This is done computationally by use of accurate pseudo-spectral techniques.

CHAPTER 2

MATHEMATICAL MODEL

2.1 Physical Problem and Governing Equations

A thin horizontal liquid layer of undisturbed dimensional thickness $2d$ is bounded by two vertical electrodes a distance $2L$ apart. The left electrode is kept at constant zero potential (without loss of generality we take the potential reference value to be zero) and a constant voltage $V = V_0$ is imposed at right electrode. In the undisturbed state, that is when the liquid layer remains of uniform thickness, the potential difference drives a horizontal electric field which is different in the liquid and the surrounding medium due to differences in the respective permittivities. We assume further that the fluid is non-conducting and that there is no free charge in the system initially. The former condition in turn implies that there will be no forces due to the field in the liquid region (such effects can be accounted for by body forces in the Navier-Stokes equations), and the latter implies that the system will remain charge-free at later times also, since no sources are present. In the present setup, then, the electric field is felt through the Maxwell stresses which supplement the viscous stresses in the normal stress balance boundary condition (see below).

The liquid layer is assumed so thin that van der Waals forces are effective. The liquid is a Newtonian viscous fluid having viscosity μ and constant density ρ . Gravity is neglected in this study, an assumption which is valid if the Bond number - the ratio of gravitational to capillary forces - is small. We are interested in modeling the dynamics of thin films and so consider the effects of attractive van der Waals forces.

We introduce a rectangular coordinate system $\mathbf{x} = (x, y)$ with associated velocity field $\mathbf{u} = (u, v)$ for the liquid. The surrounding medium is taken to be passive as regards the fluid dynamics. The interface is allowed to deform and we define $H(x, t)$

to be half of the symmetrically perturbed layer thickness; d is the half mean thickness of the layer, as introduced earlier.

The governing equations consist of the Navier-Stokes equations and the continuity equation for the fluid layer, and Laplace equations for the voltage in each phase. In what follows we denote the liquid layer by region I and the surrounding medium by region II. In terms of our coordinates, these regions are defined laterally by $0 \leq y \leq H(x, t)$ and $y \geq H(x, t)$, respectively. In dimensional form these equations are

$$\rho(u_t + uu_x + vu_y) = -(p + \Phi)_x + \mu(u_{xx} + u_{yy}), \quad (2.1)$$

$$\rho(v_t + uv_x + vv_y) = -(p + \Phi)_y + \mu(v_{xx} + v_{yy}), \quad (2.2)$$

$$u_x + v_y = 0, \quad (2.3)$$

$$V_{xx}^I + V_{yy}^I = 0, \quad (2.4)$$

$$V_{xx}^{II} + V_{yy}^{II} = 0. \quad (2.5)$$

The disjoining potential Φ has been included to model van der Waals attractive forces and this is taken to be proportional to $1/H^3$ (see for example Erneux and Davis [5]) and is defined more precisely later. Equations (2.1)-(2.5) must be solved subject to the following boundary conditions:

Symmetry conditions

$$u_y(x, 0, t) = v(x, 0, t) = 0, \quad V_y(x, 0, t) = 0. \quad (2.6)$$

Kinematic condition

$$v = H_t + uH_x, \quad \text{on } y = H(x, t) \quad (2.7)$$

Tangential stress balance on $y = H(x, t)$

$$[\underline{t} \cdot \underline{T} \cdot \underline{n}]_{II}^I = 0. \quad (2.8)$$

Normal stress balance on $y = H(x, t)$

$$\left[\underline{n} \cdot \underline{T} \cdot \underline{n} \right]_{II}^I = \frac{\sigma H_{xx}}{(1 + H_x^2)^{\frac{3}{2}}}, \quad (2.9)$$

Continuity of normal components of the electric displacement on $y = H(x, t)$

$$\underline{n} \cdot [\epsilon \underline{E}]_{II}^I = 0. \quad (2.10)$$

Continuity of tangential components of the electric field on $y = H(x, t)$

$$\underline{n} \times [\underline{E}]_{II}^I = 0. \quad (2.11)$$

Potential at infinity

$$V^{II} \rightarrow \frac{V_0}{2L} x \quad \text{as } y \rightarrow \infty. \quad (2.12)$$

In the above boundary conditions we introduce $[\ast]_{II}^I = (\ast)_I - (\ast)_{II}$. In addition, \underline{T} is the stress tensor which is made of two parts, $\underline{T} = \underline{T}_F + \underline{T}_E$, where \underline{T}_F is the fluid stress tensor and \underline{T}_E is the electrical stress tensor given below; the vectors \underline{t} and \underline{n} denote unit tangent and outward pointing normal vectors respectively, and σ is the surface tension coefficient. The unit normal and tangential vectors are given by

$$\underline{n} = \frac{1}{\sqrt{1 + H_x^2}} \begin{pmatrix} -H_x \\ 1 \end{pmatrix} \quad \text{and} \quad \underline{t} = \frac{1}{\sqrt{1 + H_x^2}} \begin{pmatrix} 1 \\ H_x \end{pmatrix}. \quad (2.13)$$

The dimensional fluid stress tensor is

$$\underline{T}_F = \begin{pmatrix} -P + 2\mu u_x & \mu(u_y + v_x) \\ \mu(u_y + v_x) & -P + 2\mu v_y \end{pmatrix}, \quad (2.14)$$

while the electric stress tensor is

$$\underline{\underline{T}}_E = \begin{pmatrix} \epsilon E_1^2 - \frac{\epsilon}{2} (E_1^2 + E_2^2) (1 - \beta) & \epsilon E_1 E_2 \\ \epsilon E_1 E_2 & \epsilon E_2^2 - \frac{\epsilon}{2} (E_1^2 + E_2^2) (1 - \beta) \end{pmatrix}, \quad (2.15)$$

where the electric field anywhere in the domain is defined by $\underline{E} = -\nabla V = (E_1, E_2)$.

Before proceeding with the nondimensionalization, we show by direct calculation that the Maxwell stresses do not contribute to the tangential stresses at the interface but instead affect normal stresses alone. We will show that $[\underline{t} \cdot \underline{\underline{T}}_E \cdot \underline{n}]_{out}^{in} = 0$. The continuity of the normal component of the displacement and the tangential component of the electric field, written out in component form in terms of the voltage potential, read (see equations (2.10) and (2.11))

$$\epsilon^{II} (V_y^{II} - H_x V_x^{II}) = \epsilon^I (V_y^I - H_x V_x^I), \quad (2.16)$$

$$H_x V_y^I + V_x^I = H_x V_y^{II} + V_x^{II}. \quad (2.17)$$

The electric contribution to the tangential stress balance equation (2.8) written out in component form, becomes

$$\begin{aligned} [\underline{t} \cdot \underline{\underline{T}}_E \cdot \underline{n}]_{II}^I &= H_x \left\{ \epsilon^I \left((V_y^I)^2 - (V_x^I)^2 \right) - \epsilon^{II} \left((V_y^{II})^2 - (V_x^{II})^2 \right) \right\} + \\ &\quad (1 - H_x^2) \left\{ \epsilon^I V_x^I V_y^I - \epsilon^{II} V_x^{II} V_y^{II} \right\}. \end{aligned} \quad (2.18)$$

Using the boundary conditions (2.16) and (2.17) into (2.18) above, verifies that

$$[\underline{t} \cdot \underline{\underline{T}}_E \cdot \underline{n}]_{II}^I = 0. \quad (2.19)$$

2.2 Nondimensionalization of the governing equations

In this section, we introduce a non-dimensionalization of the problem that will facilitate the nonlinear long wave asymptotic analysis that follow. This is done by scaling vertical coordinates with the mean film thickness d and horizontal coordinates

with the electrode separation half-distance L ; this introduces a slenderness parameter $\varepsilon = d/L$. The following scales are adopted:

$$\begin{aligned} x = Lx', \quad y = dy', \quad (u, v) = U(u', \varepsilon v'), \quad t = \frac{L}{U}t' \\ P = \rho U^2 P', \quad \Phi = \rho U^2 \Phi', \quad \text{and } V = V_0 V', \end{aligned} \quad (2.20)$$

where primed quantities denote dimensionless quantities. In what follows the primes will be dropped from the dimensionless equations. The velocity scale U is unspecified for the moment but is a typical velocity scale of the flow (for example the capillary velocity scale).

The attractive van der Waals forces appear through the potential function Φ which depends on the layer thickness and in dimensionless form is

$$\Phi = K(H_+ - H_-)^{-3}, \quad (2.21)$$

where we omit the usual additive constant (see Erneux and Davis [5]). The constant K is the non-dimensional van der Waals coefficient defined as $K = \frac{K'}{6\pi d\rho\nu^2}$ where K' is the Hamaker constant and $\nu = \mu/\rho$ is the kinematic viscosity. Using the symmetry condition $H_+(x, t) = -H_-(x, t)$ and writing $H_+ = H(x, t)$, we get

$$\Phi = \frac{K}{8H^3}. \quad (2.22)$$

Substitution of the scales (2.20) into the governing equations (2.1)-(2.5) and boundary conditions (2.6)-(2.12) and dropping of the primes, provides the dimensionless system to be solved. Before writing these equations down, we introduce a voltage perturbation \tilde{V} defined through

$$V^{I,II} = \frac{x}{2} + \tilde{V}^{I,II}. \quad (2.23)$$

The first term in (2.23) comes from the undisturbed part of the voltage drop across the electrodes and the perturbation is arbitrary in the formulation that follows. The dimensionless equations and boundary conditions become, then:

Navier-Stokes equations

$$u_t + uu_x + vv_y = -(P + \Phi)_x + \frac{1}{Re}(u_{xx} + \frac{1}{\varepsilon^2}u_{yy}), \quad (2.24)$$

$$\varepsilon^2(v_t + uv_x + vv_y) = -(P + \Phi)_y + \frac{\varepsilon^2}{Re}(v_{xx} + \frac{1}{\varepsilon^2}v_{yy}), \quad (2.25)$$

$$u_x + v_y = 0 \quad (2.26)$$

where $Re = \frac{\rho UL}{\mu}$ is the Reynold number.

Voltage potential

$$\varepsilon^2\tilde{V}_{xx}^I + \tilde{V}_{yy}^I = 0. \quad (2.27)$$

$$\varepsilon^2\tilde{V}_{xx}^{II} + \tilde{V}_{yy}^{II} = 0. \quad (2.28)$$

The boundary conditions, written out in component form have the following non-dimensional forms.

Symmetry conditions

$$u_y(x, 0, t) = v(x, 0, t) = 0, \quad \tilde{V}_y^I(x, 0, t) = 0. \quad (2.29)$$

Kinematic condition

$$v = H_t + uH_x, \quad \text{on } y = H(x, t) \quad (2.30)$$

Tangential stress balance on $y = H(x, t)$

$$2\varepsilon^2 H_x (v_y - u_x) + (1 - \varepsilon^2 H_x^2) (u_y + \varepsilon^2 v_x) = 0. \quad (2.31)$$

Normal stress balance on $y = H(x, t)$

$$-P + \frac{1}{1 + \varepsilon^2 H_x^2} \left\{ \frac{2}{Re} u_x (\varepsilon^2 H_x^2 - 1) - \frac{2}{Re} H_x (u_y + \varepsilon^2 v_x) \right\} +$$

$$\begin{aligned}
& \frac{1}{1 + \varepsilon^2 H_x^2} \frac{\bar{E}_b}{\varepsilon} \left\{ \varepsilon^2 H_x^2 \left[\frac{\varepsilon}{2}(1 + \beta) \left(\frac{1}{4} + \tilde{V}_x + \tilde{V}_x^2 \right) - \frac{\varepsilon}{2}(1 - \beta) \frac{\tilde{V}_y^2}{\varepsilon^2} \right]_{II}^I - \right. \\
& \left. 2H_x \left[\varepsilon \left(\frac{1}{2} + \tilde{V}_x \right) \tilde{V}_y \right]_{II}^I + \left[\frac{\varepsilon}{2}(1 + \beta) \frac{\tilde{V}_y^2}{\varepsilon^2} - \frac{\varepsilon}{2}(1 - \beta) \left(\frac{1}{4} + \tilde{V}_x + \tilde{V}_x^2 \right) \right]_{II}^I \right\} \\
& = \frac{\varepsilon}{CaRe} \frac{H_{xx}}{(1 + \varepsilon^2 H_x^2)^{\frac{3}{2}}} \text{ at } y = H, \quad (2.32)
\end{aligned}$$

where $Ca = \frac{\mu U}{\sigma}$ is the capillary number which will be taken to be small in the sequel, in order to retain the effects of surface tension to leading order. The electric capillary number $E_b = \frac{V_0^2}{L^2} \frac{1}{\rho U^2}$ is the ratio of electrically induced pressure to fluid pressure.

Continuity of normal components of the electric displacement on $y = H(x, t)$

$$\epsilon_p \left[\varepsilon^2 H_x \left(\frac{1}{2} + \tilde{V}_x^I \right) - \tilde{V}_y^I \right] = \varepsilon^2 H_x \left(\frac{1}{2} + \tilde{V}_x^{II} \right) - \tilde{V}_y^{II}, \quad (2.33)$$

where $\epsilon_p = \frac{\varepsilon^I}{\varepsilon^{II}} (> 1)$ is the relative permittivity. In applications with air as a surrounding medium, $\varepsilon^{II} = \varepsilon_o$, the free-space permittivity.

Continuity of tangential components of the electric field on $y = H(x, t)$

$$H_x \tilde{V}_y^I + \tilde{V}_x^I = H_x \tilde{V}_y^{II} + \tilde{V}_x^{II}. \quad (2.34)$$

Potential at infinity

$$\tilde{V}^{II} \rightarrow 0 \quad \text{as } y \rightarrow \infty. \quad (2.35)$$

Finally, we summarize the dimensionless groups that appear in the equations. These are the Reynolds number Re , the Capillary number Ca , the relative permittivity ϵ_p and the electric capillary number E_b :

$$Re = \frac{\rho U L}{\mu}, \quad Ca = \frac{\mu U}{\sigma}, \quad \epsilon_p = \frac{\varepsilon^I}{\varepsilon_o}, \quad E_b = \frac{V_0^2}{L^2} \frac{1}{\rho U^2}. \quad (2.36)$$

The dimensionless problem given above, supplied with appropriate initial and boundary conditions, constitutes a nonlinear free-surface system whose evolution can

terminate in finite-time singularities. The scalings introduced above can be thought of as exact transformations; in particular, the case $\varepsilon = 1$ recovers the system when the vertical and horizontal scales are not disparate.

In Chapter 2, we develop the linear stability of the full system treating ε as an order one parameter. The limit $\varepsilon \ll 1$ corresponds to long waves in the sense of shallow wave theory. Later, we consider the nonlinear evolution of such long waves and develop a system of evolution equations. The linear stability of the evolution equations recovers the $\varepsilon \ll 1$ limit of the linear stability of the full system, as expected.

CHAPTER 3

LINEAR STABILITY

3.1 Derivation of the Linear Stability Equations

The flow is incompressible and two-dimensional and so we can introduce a stream function ψ such that $u = \psi_y$ and $v = -\psi_x$. This satisfies (1.4) identically and after the elimination of $P + \Phi$ from the momentum equations (2.24) and (2.25), we obtain the following nonlinear equation for the stream function:

$$\psi_{yyt} + \varepsilon^2 \psi_{xxt} + \psi_y(\psi_{yyx} + \varepsilon^2 \psi_{xxx}) - \psi_x(\psi_{yyy} + \varepsilon^2 \psi_{xxy}) = \frac{1}{Re} \left(\frac{1}{\varepsilon^2} \psi_{yyyy} + 2\psi_{xxyy} + \varepsilon^2 \psi_{xxxx} \right). \quad (3.1)$$

Equation (3.1) can be used instead of the two momentum equations and the continuity equation.

We are interested in studying the stability of the baseflow to disturbances which are periodic in the x -direction and of wavenumber k . The underlying flow consists of the flat stationary liquid layer with a uniform horizontal electric field acting. The stream function, interface and voltage potentials are perturbed as follows:

$$(\psi, H, \tilde{V}^{I,II}, P) = (\delta \hat{\psi}(y), 1 + \delta H_0, \delta \hat{V}^{I,II}(y), P_0 + \delta \hat{P}(y)) \exp(ikx + \omega t), \quad (3.2)$$

where $0 < \delta \ll 1$ is a linearization amplitude. Substitution of (3.2) into the dimensionless governing equations (3.1), (2.27), (2.28) as well as the boundary conditions (2.29)-(2.35), and keeping order δ terms alone, provides the following boundary value problem for the y -dependent eigenfunctions:

$$\hat{\psi}^{(4)} - \hat{\psi}'' (2k^2 \varepsilon^2 + \varepsilon^2 \omega Re) + \hat{\psi} (\varepsilon^4 k^4 + \varepsilon^4 k^2 \omega Re) = 0, \quad (3.3)$$

$$\frac{d^2 \hat{V}^{I,II}}{dy^2} - k^2 \hat{V}^{I,II} = 0, \quad (3.4)$$

Symmetry condition

$$\hat{\psi}(0) = \hat{\psi}'(0) = 0, \quad \frac{d\hat{V}^I}{dy}(0) = 0 \quad (3.5)$$

Kinematic condition

$$-ik\hat{\psi}(1) = \omega H_0 \quad (3.6)$$

Tangential stress balance

$$\frac{d^2\hat{\psi}}{dy^2}(1) + \varepsilon^2 k^2 \hat{\psi}(1) = 0 \quad (3.7)$$

Normal stress balance

$$-\hat{P}(1) - \frac{2ik}{Re}\hat{\psi}'(1) - \frac{ik}{2} \frac{\bar{E}_b}{\varepsilon} (\hat{V}^I(1) - \hat{V}^{II}(1)) = -\frac{\varepsilon}{CaRe} k^2 H_0 \quad (3.8)$$

Continuity of normal components of the electric displacement

$$\frac{ik}{2} \varepsilon^2 (\varepsilon_p - 1) H_0 = \varepsilon_p \frac{d\hat{V}^I}{dy}(1) - \frac{d\hat{V}^I}{dy}(1) \quad (3.9)$$

Continuity of tangential components of the electric field

$$\hat{V}^I(1) = \hat{V}^{II}(1) \quad (3.10)$$

Potential at infinity

$$\hat{V}^{II} \rightarrow 0 \quad \text{as } y \rightarrow \infty. \quad (3.11)$$

The solution of this eigenvalue problem and the derivation of the dispersion relation that provides the growth rates of different wavelength disturbances, is pursued next.

3.2 Solution of the Linear Problem and the Dispersion Relation

The solution of (3.3) subject to the conditions (3.5) at $y = 0$ is

$$\hat{\psi}(y) = A \sinh(\varepsilon y \sqrt{k^2 + \omega Re}) + D \sinh(\varepsilon ky). \quad (3.12)$$

The constant D appearing in the solution (3.12) above, can be expressed in terms of A through use of the tangential stress balance condition (3.7). The result is

$$\hat{\psi}(y) = e^{ikx + \omega t} A \left\{ \sinh(\varepsilon y \sqrt{k^2 + \omega Re}) - \frac{(2k^2 + \omega Re) \sinh(\varepsilon \sqrt{k^2 + \omega Re})}{2k^2 \sinh(\varepsilon k)} \sinh(\varepsilon ky) \right\}. \quad (3.13)$$

The normal stress balance usually provides the second equation required to obtain the eigenrelation. In the presence of electric fields, however, the presence of electrical normal stresses necessitates solution of the voltage equations first. These solutions are found from (3.4) and are given by

$$\hat{V}^I(y) = B \cosh(\varepsilon ky), \quad \hat{V}^{II}(y) = C \exp(-\varepsilon ky), \quad (3.14)$$

where the boundary conditions (3.5) and (3.11) have been used.

The linearized normal stress condition (3.8) contains the pressure perturbation $\hat{P}(1)$. An expression for this that can then be used into the normal stress balance condition, can be found by considering the linearized x -momentum equation. Starting from (2.24) and noting that the linearization of the disjoining pressure equation (2.21) is $-\frac{3}{8}K\delta H_0 \exp(ikx + \omega t)$, yields

$$ik\hat{P}(1) = \frac{3}{8}ikKH_0 - \omega\hat{\psi}'(1) + \frac{1}{Re} \left(-k^2\hat{\psi}'(1) + \frac{1}{\varepsilon^2}\hat{\psi}'''(1) \right). \quad (3.15)$$

Equation (3.15) shows that $\hat{P}(1)$ can be expressed in terms of an expression involving the constants A and H_0 . The latter can now be found in terms of A by consideration of the linearized kinematic condition (3.6) and use of the solution (3.13) for $\hat{\psi}$. The

result is

$$H_0 = \frac{iARe \sinh(\varepsilon\sqrt{k^2 + \omega Re})}{2k}. \quad (3.16)$$

These calculations show that the normal stress boundary condition (3.8) can be written to contain the constants A , B and C alone, the latter two coming from the voltage solutions (3.14).

We can express C in terms of B by consideration of the continuity of the tangential components of the electric field across the interface (see equation (3.10)). Using (3.14) into (3.10), then, yields

$$B \cosh(\varepsilon k) = C \exp(-\varepsilon k). \quad (3.17)$$

This in turn enables expression of the normal stress balance boundary condition (3.8) so that the constants A and B alone appear. This equation is

$$\begin{aligned} & A \left\{ \omega \varepsilon \left[\sqrt{k^2 + \omega Re} \cosh(\varepsilon\sqrt{k^2 + \omega Re}) - \right. \right. \\ & \quad \left. \left. \frac{(2k^2 + \omega Re)}{2k} \sinh(\varepsilon\sqrt{k^2 + \omega Re}) \coth(\varepsilon k) \right] + \right. \\ & \quad \varepsilon \left[\left(\frac{2k^2}{Re} - \omega \right) \sqrt{k^2 + \omega Re} \cosh(\varepsilon\sqrt{k^2 + \omega Re}) - \right. \\ & \quad \quad \left. \left(\frac{2k^3}{Re} + \omega k \right) \sinh(\varepsilon\sqrt{k^2 + \omega Re}) \coth(\varepsilon k) - \right. \\ & \quad \left. \left. \frac{\sigma}{\rho U^2 L} \frac{k^2}{2} Re \sinh(\varepsilon\sqrt{k^2 + \omega Re}) \right] + \frac{3}{16} Re K \sinh(\varepsilon\sqrt{k^2 + \omega Re}) \right\} \\ & + B \left\{ \frac{1}{\rho U^2} \frac{V_0^2}{L^2} \frac{\epsilon_o}{2} k^2 \cosh(\varepsilon k) [\epsilon_p(1 - \beta) - 1] \right\} = 0. \quad (3.18) \end{aligned}$$

A second equation involving A and B is found by using the continuity of the normal component of the electric displacement across the interface, equation (3.9).

This yields

$$\frac{\varepsilon}{2}(\epsilon_p - 1)ikH_0 = \epsilon_p kB \sinh(\varepsilon k) + Ck \exp(-\varepsilon k), \quad (3.19)$$

which on use of (3.16) and (3.17) to eliminate H_0 and C , becomes

$$A \left\{ \frac{\varepsilon}{4} (\epsilon_p - 1) Re \sinh(\varepsilon \sqrt{k^2 + \omega Re}) \right\} + Bk \{ \epsilon_p \sinh(\varepsilon k) + \cosh(\varepsilon k) \} = 0. \quad (3.20)$$

The homogeneous equations (3.18) and (3.20) have non-trivial solutions if the following expression, the dispersion relation, is satisfied

$$\begin{aligned} \omega^2 + 4 \frac{\omega k^2}{Re} - 4 \frac{k^3}{Re^2} \sqrt{k^2 + \omega Re} \coth(\varepsilon \sqrt{k^2 + \omega Re}) \tanh(\varepsilon k) + \\ 4 \frac{k^4}{Re^2} + \frac{1}{CaRe} k^3 \tanh(\varepsilon k) - \frac{3 k K}{8 \varepsilon} \tanh(\varepsilon k) + \\ \frac{E_b \epsilon_o k^2 \sinh(\varepsilon k) (\epsilon_p - 1)^2}{4(\epsilon_p \sinh(\varepsilon k) + \cosh(\varepsilon k))} = 0. \end{aligned} \quad (3.21)$$

This equation must be solved to obtain $\omega(k)$ and instability results if $Real(\omega) > 0$. The equation is implicit for ω and in fact an infinite number of solutions are possible for each k - this follows from the transcendental nature of the equation. The objective is to determine the value(s) of k which provide the most unstable waves with the maximum growth rate. Solutions are obtained numerically using root-finding methods.

The effect of the electric field on the stability in this case, is shown in Figure 3.1. Here the van der Waals parameter is $K = 80$ and the dimensionless electric field parameter E_b ranges from 0 to 2,000. We see that as the strength of the electric field increases, the maximum growth rate decreases and the most unstable wave length increases; at the same time the wave number cut off decreases.

Figure 3.2 shows the effect of the slenderness parameter ε on the stability. Results are shown for fixed values of $K = 80$, $S = \frac{\varepsilon}{CaRe} = 50$ (S is a surface tension parameter) and $V = E_b = 50$, as ε varies from 0.5 to 1.0. We see that the stability is enhanced as ε increases, with the band of unstable modes increasing with decreasing ε .

The stability characteristics are considered in a more collective form next. Here we produce two-dimensional surface plots to capture essential features as the van der

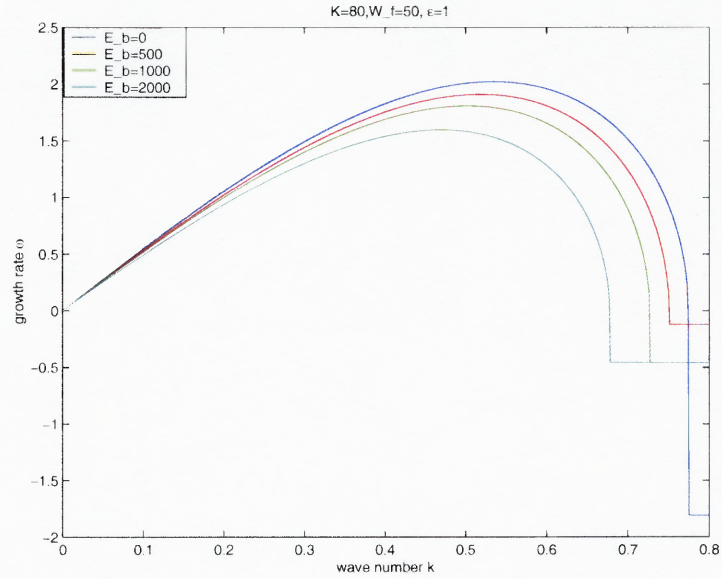


Figure 3.1 The relation between wave number k and growth rates ω with different E_b in equation (3.21)

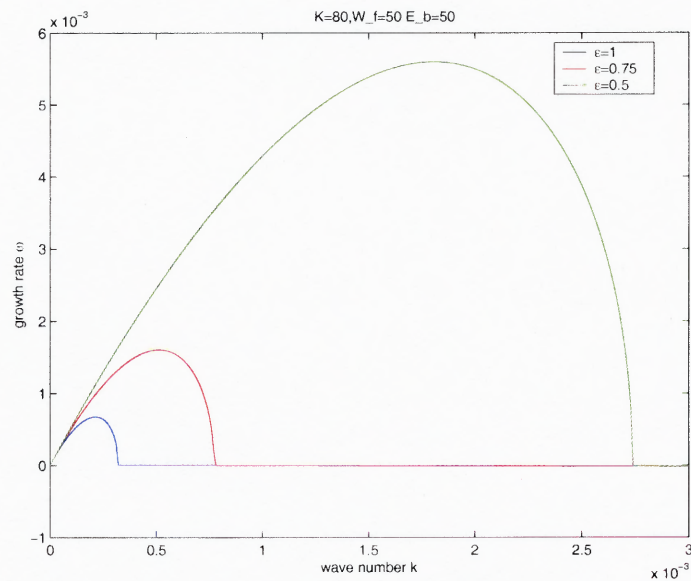


Figure 3.2 The relation between wave number k and growth rate ω for different ε in equation (3.21)

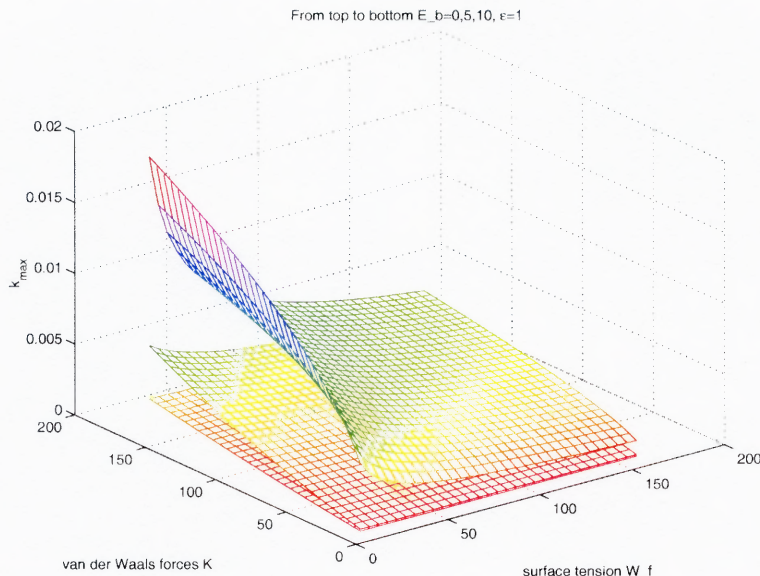


Figure 3.3 The relation between van der Waals forces, surface tension and k_{max} for different V in equation (3.21)

Waals parameter K (or A in the Figures) and the surface tension parameter S , vary. The first set of results is produced by fixing $\epsilon = 1.0$ and for three different values of $E_b = 0, 5, 10$. Results are given in Figures 3.3 and 3.4.

Figure 3.3 shows the wave number of the maximally growing wave as K and S vary over positive values. Enhanced stability is observed once again as the electric field is increased. The lowest of the three surfaces has $E_b = 10$ and produces the smallest values of k_{max} and hence is the most stable situation.

Figure 3.4 gives the corresponding results for the critical wave number, k_{cut} , below which the flow is stable, that is all disturbances with wavelengths shorter than $2\pi/k_{cut}$ are stable. The top surface corresponds to no electric field ($E_b = 0$). As the electric field is increased the surfaces move down monotonically, implying uniformly enhanced stability.

The case of a fixed electric field and variations in the slenderness ratio ϵ are considered next. We present stability results in Figures 3.5 and 3.6 for a range of

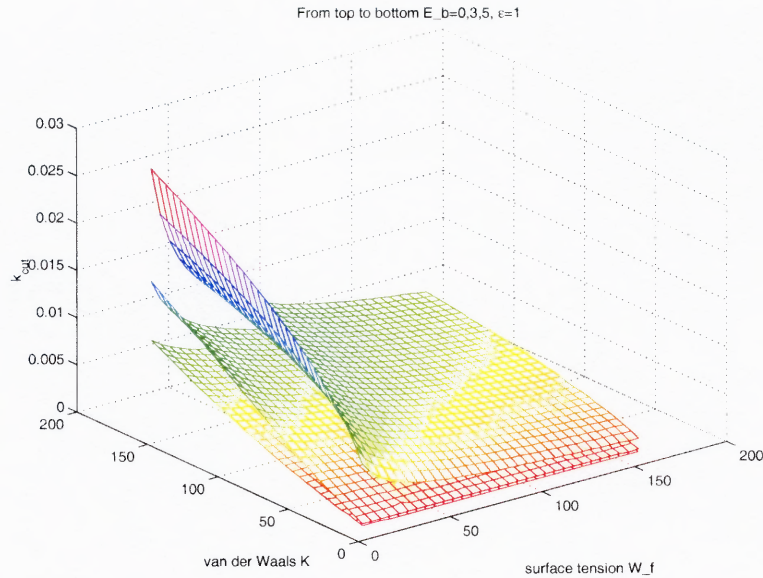


Figure 3.4 The relation between van der Waals forces, surface tension and k_{cut} for different E_b in equation (3.21)

values of ε between 0.5 and 1.0. Figure 3.5 shows the behavior of k_{max} as K and S are varied, while Figure 3.6 shows the corresponding behavior for the critical wavenumber k_{cut} . It is seen that as ε increases, the flow becomes uniformly more stable for the large range of K and S considered in the Figures.

It can be concluded from these results, therefore, that surface tension acts to stabilize the flow for a given van der Waals parameter K . We are not particularly concerned with short wave disturbances since these will be damped by viscosity even in the absence of surface tension. What is more interesting is the general effects of the three different competing mechanisms of van der Waals forces that contribute to the instability, and surface tension and electric field forces which exert a stabilizing influence. Figures 3.1 - 3.6 show that given a van der Waals parameter K , an electric capillary number E_b can be found so that the flow is stabilized (linearly at least). The implicit form of the dispersion relation (3.21) does not provide a simple expression that can be used to make this conclusion and numerical solutions like the ones included

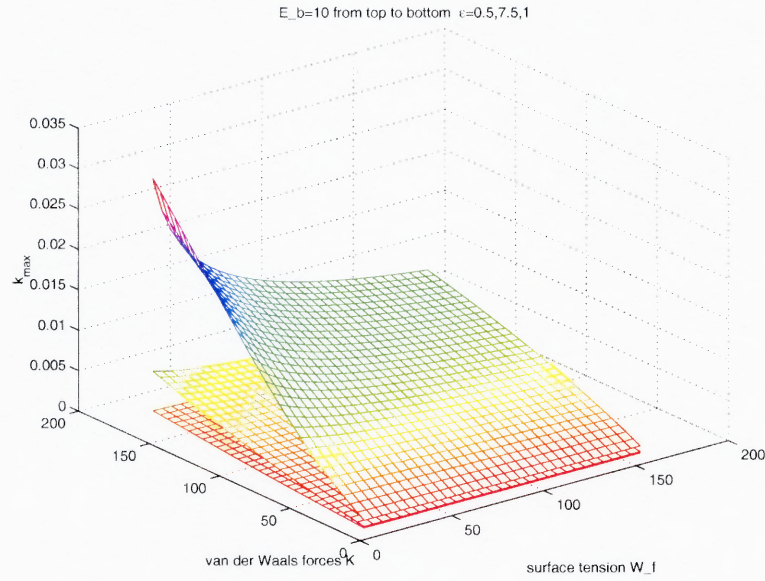


Figure 3.5 The relation between van der Waals forces, surface tension and k_{max} for different ϵ in equation (3.21)

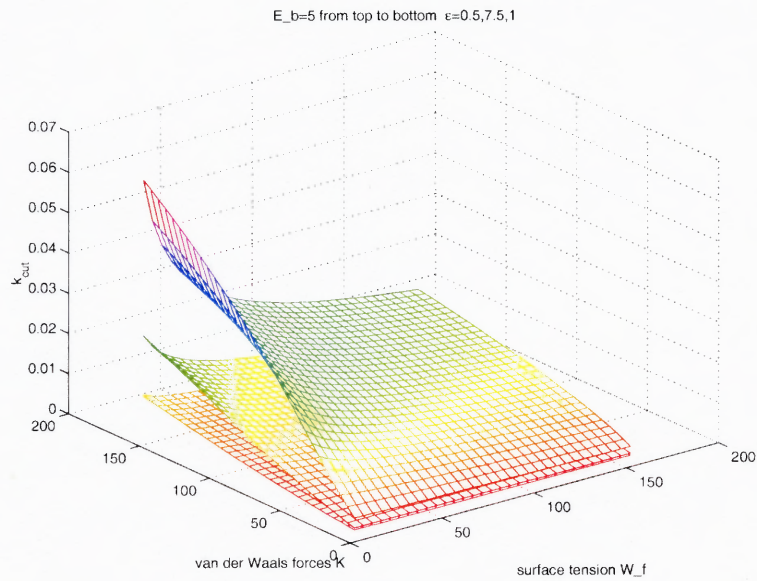


Figure 3.6 The relation between van der Waals forces, surface tension and k_{cut} for different ϵ in equation (3.21)

here, are necessary. The long wave theory presented in Chapter 4 elucidates this point much more due to the closed form expressions for $\omega(k)$ which are possible in that case. We will also use the nonlinear system to evaluate the long time dynamics near such stability thresholds.

3.3 Asymptotic Results For Small ε And Scales For The Nonlinear Theory

In this section, we present some asymptotic results of the dispersion relation (3.21) and in particular consider the slenderness limit $\varepsilon \rightarrow 0$. This is the appropriate limit for comparisons with the linear stability of the nonlinear long wave models we derive in Chapter 4. In addition, this analysis helps to identify the scalings required for the nonlinear development which is based on strong surface tension (small capillary numbers) and strong electric fields (large electric capillary numbers).

Starting from (3.21), then, we need to consider expansions of the various terms for small ε and keeping all non-dimensional groups as order one variables, for the time being. This can be done in a straightforward manner; only the third term in (3.21) requires some attention and is first written as

$$-\frac{4k^3}{Re^2} \frac{1}{\varepsilon} \varepsilon \sqrt{k^2 + \omega Re} \coth(\varepsilon \sqrt{k^2 + \omega Re}) \tanh(\varepsilon k). \quad (3.22)$$

Using the fact that $\alpha \coth(\alpha) = 1 + O(\alpha)$ as $\alpha \rightarrow 0$ and identifying $\alpha = \varepsilon \sqrt{k^2 + \omega Re}$ in (3.22), gives the following leading order dispersion relation valid for slender geometries

$$\omega^2 + \frac{4}{Re} k^2 \omega - \frac{3}{8} K k^2 + \frac{\varepsilon_0 (\varepsilon_p - 1)^2 \varepsilon E_b}{4} k^2 |k| + \frac{\varepsilon}{Ca Re} k^4 = 0. \quad (3.23)$$

If we take Re to be an order one quantity, then we observe from (3.23) that surface tension and electric field effects will be retained in this limit as long as

$$Ca \sim \varepsilon, \quad E_b \sim 1/\varepsilon. \quad (3.24)$$

These are precisely the scales used in Chapter 4 to capture the leading order nonlinear evolution of this flow when surface tension and electric field effects are present.

The long wave nonlinear problem in the absence of an electric field has been studied by Erneux and Davis [5]. For completeness we consider the generation of their dispersion relation by starting with our equation (3.23). The key to achieving this is to note the differences in non-dimensionalization. Erneux and Davis (ED from now on) use $2d$ as the scale for lengths, $\nu/2d$ as the velocity scale, $4d^2/\nu$ to scale time and $\rho\nu^2/4d^2$ for the pressure scale. This implies that our Reynolds number $Re = 1/\varepsilon$ which casts (3.23) with $E_b = 0$ into

$$\omega^2 + 4\varepsilon k^2 \omega - \frac{3}{8} K k^2 + \frac{\varepsilon^2}{Ca} k^4 = 0. \quad (3.25)$$

The changes in scales due to the different non-dimensionalizations can be used to obtain the ED dispersion relation from (3.25). More specifically, if we transform according to

$$\omega \rightarrow \frac{\omega}{\varepsilon}, \quad k \rightarrow \frac{k}{\varepsilon}, \quad Ca \rightarrow \frac{2}{3S},$$

the relation (3.25) recovers that of Erneux and Davis [5].

CHAPTER 4

NONLINEAR STABILITY

4.1 Derivation Of The Nonlinear Evolution Equations

The objective of this section is to study the nonlinear stability of flows in the electrified viscous film by using asymptotic methods in the limit $\varepsilon \rightarrow 0$. The governing equations and boundary conditions can be found in Section 2.2 and comprise of the Navier-Stokes and Laplace equations for the fluid and voltage potential respectively (equations (2.24)-(2.28), and the boundary conditions (2.29)-(2.35). As has been argued in Section 3.3, the distinguished limits given by (3.24) must be used in order to retain surface tension and electric field effects. This can also be seen from the normal stress balance boundary condition (2.32) and consideration of leading order terms in an asymptotic expansion in ε . In what follows, then, we define

$$Ca = \frac{\varepsilon}{\Sigma}, \quad E_b = \frac{\bar{E}_b}{\varepsilon}, \quad (4.1)$$

where Σ and \bar{E}_b are order one quantities. In addition, Re is an order one quantity which, as we see later, can be scaled out of the problem. With these scales, the normal stress boundary condition at $y = H(x, t)$, becomes

$$\begin{aligned} & -P + \frac{1}{1 + \varepsilon^2 H_x^2} \left\{ \frac{2}{Re} u_x (\varepsilon^2 H_x^2 - 1) - \frac{2}{Re} H_x (u_y + \varepsilon^2 v_x) \right\} + \\ & \frac{1}{1 + \varepsilon^2 H_x^2} \frac{\bar{E}_b}{\varepsilon} \left\{ \varepsilon^2 H_x^2 \left[\frac{\varepsilon}{2} (\tilde{V}_x + \tilde{V}_x^2) - \frac{\varepsilon}{2} \frac{\tilde{V}_y^2}{\varepsilon^2} \right]_{II}^I - \right. \\ & \left. 2H_x \left[\varepsilon (\tilde{V}_x) \tilde{V}_y \right]_{II}^I + \left[\frac{\varepsilon}{2} \frac{\tilde{V}_y^2}{\varepsilon^2} - \frac{\varepsilon}{2} (\tilde{V}_x + \tilde{V}_x^2) \right]_{II}^I \right\} \\ & = \frac{\Sigma}{Re} \frac{H_{xx}}{(1 + \varepsilon^2 H_x^2)^{\frac{3}{2}}}. \end{aligned} \quad (4.2)$$

We begin our analysis by construction of the electric potential solutions in regions I and II , that is inside and outside the fluid sheet. An asymptotic solution

is sought in the form

$$\tilde{V}^{I,II} = \varepsilon \tilde{V}_1^{I,II} + \varepsilon^2 \tilde{V}_2^{I,II} + \dots \quad (4.3)$$

Some comments regarding this expansion are in order. First, note that we are looking for a solution which is a correction to the base voltage potential (equal to $\frac{x}{2}$ in dimensionless terms). The size of this correction is of order ε , i.e. of the same order as the deflection amplitude of the free fluid interface, and this is reflected in (4.3). Substitution of (4.3) into the Laplace equations (2.27) and (2.28) gives, to leading order

$$\tilde{V}_{1yy}^{I,II} = 0, \quad (4.4)$$

which when integrated twice and use is made of the symmetry conditions (2.29) along with the condition at infinity (2.35), gives

$$\tilde{V}_1^I = \chi(x, t), \quad (4.5)$$

$$\tilde{V}_1^{II} = \chi^*(x, t), \quad (4.6)$$

where χ and χ^* are to be found. At the next order, we have

$$\tilde{V}_{2yy}^{I,II} = 0, \quad (4.7)$$

which on integration and use of the symmetry conditions for the solution in region I , gives

$$\tilde{V}_2^I = a(x, t), \quad (4.8)$$

$$\tilde{V}_2^{II} = A(x, t) + yB(x, t). \quad (4.9)$$

The functions appearing in (4.8) and (4.9) above, need to be determined by the boundary conditions at the interface; the conditions at infinity must also be satisfied.

The latter is seen to be problematic due to the algebraic growth of \tilde{V}_2^{II} for large y . This necessitates the introduction of an outer region and matching between the two, as explained later on.

Let us consider the electric field boundary conditions next, at each order in ε . The non-dimensional normal electric field displacement condition at $y = H(x, t)$ has been given in Section 2.2 and reads

$$\epsilon_p \left(\varepsilon^2 H_x \left(\frac{1}{2} + \tilde{V}_x^I \right) - \tilde{V}_y^I \right) = \varepsilon^2 H_x \left(\frac{1}{2} + \tilde{V}_x^{II} \right) - \tilde{V}_y^{II}$$

where $\epsilon^I = \epsilon_o \epsilon_p$ and $\epsilon^{II} = \epsilon_o$. At $O(\varepsilon)$ we get

$$-\epsilon_p \tilde{V}_{1y}^I = -\tilde{V}_{1y}^{II}, \quad \text{at } y = H(x, t). \quad (4.10)$$

This boundary condition is seen to be satisfied identically by the leading order solutions (4.5) and (4.6). At $O(\varepsilon^2)$ we have

$$\epsilon_p \left(\frac{H_x}{2} - \tilde{V}_{2y}^I \right) = \frac{H_x}{2} - \tilde{V}_{2y}^{II}, \quad \text{at } y = H(x, t), \quad (4.11)$$

which implies that

$$B(x, t) = \frac{H_x}{2} (1 - \epsilon_p). \quad (4.12)$$

Consider continuity of the tangential component of the electric field, next. This is

$$H_x \tilde{V}_y^{II} + \tilde{V}_x^{II} = H_x \tilde{V}_y^I + \tilde{V}_x^I, \quad \text{at } y = H(x, t),$$

and to leading order it gives

$$H_x \tilde{V}_{1y}^{II} + \tilde{V}_{1x}^{II} = H_x \tilde{V}_{1y}^I + \tilde{V}_{1x}^I, \quad \text{at } y = H(x, t), \quad (4.13)$$

which in turn relates the function χ and χ^* through

$$\chi_x = \chi_x^*.$$

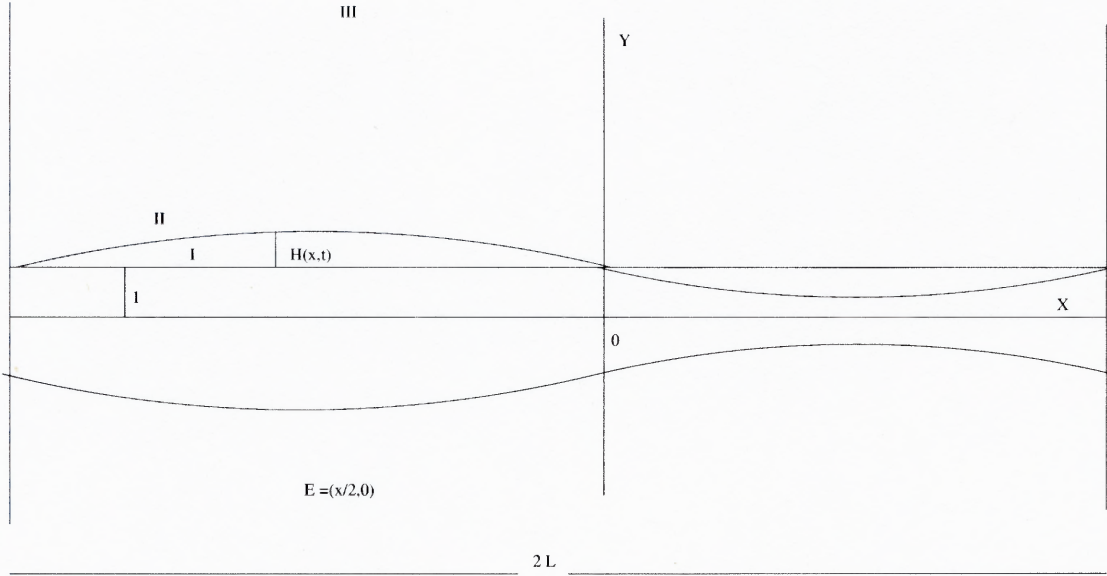


Figure 4.1 The three regions for the asymptotic solution.

We choose the integration constant to be 0, and so

$$\chi(x, t) = \chi^*(x, t). \quad (4.14)$$

At the next order, $o(\varepsilon^2)$, we obtain from this boundary condition,

$$H_x \tilde{V}_{2y}^{II} + \tilde{V}_{2x}^{II} = H_x \tilde{V}_{2y}^I + \tilde{V}_{2x}^I, \quad \text{at } y = H(x, t),$$

which in turn relates the functions a , A and B through

$$a(x, t) = A(x, t) + H(x, t)B(x, t). \quad (4.15)$$

Summarizing, then, we have two leading orders

$$\tilde{V}^I = \varepsilon \chi + \varepsilon^2 \left(A + H \frac{H_x}{2} (1 - \epsilon_p) \right) + \dots \quad (4.16)$$

$$\tilde{V}^{II} = \varepsilon \chi + \varepsilon^2 \left(A + y \frac{H_x}{2} (1 - \epsilon_p) \right) + \dots \quad (4.17)$$

As mentioned earlier, the asymptotic solution \tilde{V}^{II} breaks down as $y \rightarrow \infty$; the boundary condition of decay to zero at infinity is not possible, and in fact all terms in

asymptotic series become of the same order when $y \sim \varepsilon^{-1}$. This suggests scaling on this variable and introducing an outer region *III*, say, where $x = X$ and $y = \frac{Y}{\varepsilon}$ (X and Y are now order one independent variables). A schematic of the three regions to be considered is given in Figure 4.1. Once the outer solution in region *III* is found, it must satisfy the boundary condition (2.12) far away as $Y \rightarrow \infty$, and also must match with the inner solution in region *II* as $Y \rightarrow 0$ (details of this matching procedure are given later). The expansion in region *III* is

$$\tilde{V}^{III} = \varepsilon \tilde{V}_1^{III} + \varepsilon^2 \tilde{V}_2^{III} + \dots \quad (4.18)$$

The full Laplace equation needs to be addressed in region *III*, i.e., we need to solve

$$\tilde{V}_{XX}^{III} + \tilde{V}_{YY}^{III} = 0, \quad (4.19)$$

with the boundary condition $\tilde{V}^{III} \rightarrow 0$ as $Y \rightarrow \infty$. Defining Fourier transforms by $\hat{f} = \mathcal{F}(f) = \int_{-\infty}^{\infty} f(X, Y, t) e^{-ikX} dX$ we obtain the following problems at each order in ε in Fourier space:

$$-k^2 \hat{\tilde{V}}_{iXX}^{III} + \hat{\tilde{V}}_{iYY}^{III} = 0, \quad \text{for } i = 1, 2, \dots,$$

whose solutions which satisfy the boundary conditions at infinity are

$$\hat{\tilde{V}}_i^{III} = \alpha_i(X, t) \exp(-|k|Y). \quad (4.20)$$

The solution for the voltage potential in region *III* takes the following form,

$$\hat{V}^{III} = \varepsilon \alpha_1(X, t) e^{-|k|Y} + \varepsilon^2 \alpha_2(X, t) e^{-|k|Y} + \dots, \quad (4.21)$$

and as $Y \rightarrow 0$, this must be matched with the solution coming out of region *II*. To achieve this, we consider the Fourier transform of \tilde{V}^{II} , yielding,

$$\mathcal{F}(\tilde{V}^{II}) = \varepsilon \hat{\chi} + \varepsilon^2 \left(\hat{A} + y \frac{(1 - \epsilon_p)}{2} ik \hat{H} \right) + \dots \quad (4.22)$$

Asymptotic matching requires that we equate the following expressions,

$$\lim_{Y \rightarrow \infty} \mathcal{F}(\tilde{V}^{II}) = \varepsilon \hat{\chi} + \varepsilon \frac{Y}{2} (1 - \epsilon_p) i k \hat{H} + \varepsilon^2 \hat{A} + \dots, \quad (4.23)$$

$$\lim_{Y \rightarrow 0} \hat{V}^{III} = \varepsilon \alpha_1 (1 - |k|Y + k^2 Y^2 + \dots) + \varepsilon^2 \alpha_2 (1 - |k|Y + k^2 Y^2 + \dots) + \dots \quad (4.24)$$

It is useful, in what follows, to introduce the Hilbert transform operator, \mathcal{H} , defined by

$$\mathcal{H}(f(x)) = \frac{1}{\pi} PV \int_{-\infty}^{\infty} \frac{f(y)}{x - y} dy, \quad (4.25)$$

where PV denotes the principal value of the integral. Then the leading order matching closes the problem, and we calculate,

$$\alpha_1 = \hat{\chi}, \quad (4.26)$$

$$\alpha_2 = \hat{A}, \quad (4.27)$$

$$-\alpha_1 |k| = \frac{(1 - \epsilon_p)}{2} i k \hat{H}. \quad (4.28)$$

Therefore,

$$\chi(x, t) = \frac{(1 - \epsilon_p)}{2} \mathcal{H}(H). \quad (4.29)$$

With these expressions available, we can summarize a few terms in the asymptotic series of the solution in regions I and II as follows:

$$V^I = \frac{x}{2} + \varepsilon \frac{1 - \epsilon_p}{2} \mathcal{H}(H) + \varepsilon^2 \left(A + H \frac{H_x}{2} (1 - \epsilon_p) \right) + \dots \quad (4.30)$$

$$V^{II} = \frac{x}{2} + \varepsilon \frac{1 - \epsilon_p}{2} \mathcal{H}(H) + \varepsilon^2 \left(A + y \frac{H_x}{2} (1 - \epsilon_p) \right) + \dots \quad (4.31)$$

Next, we turn to the asymptotic solution for the fluid dynamics problem. Expanding as before, we have

$$u = u_0 + \varepsilon u_1 + \varepsilon^2 u_2 + \dots, \quad (4.32)$$

$$v = v_0 + \varepsilon v_1 + \varepsilon^2 v_2 + \dots, \quad (4.33)$$

$$P = P_0 + \varepsilon P_1 + \varepsilon^2 P_2 + \dots, \quad (4.34)$$

$$\Phi = \Phi_0 + \varepsilon \Phi_1 + \varepsilon^2 \Phi_2 + \dots \quad (4.35)$$

With $Re = O(1)$, the leading order equations from the Navier-Stokes are

$$u_{0yy} = 0, \quad (4.36)$$

$$\frac{1}{Re} v_{0yy} = (P_0 + \Phi_0)_y, \quad (4.37)$$

$$u_{0x} + v_{0y} = 0. \quad (4.38)$$

The leading order contribution from the tangential stress balance equation is

$$u_{0y} = 0, \quad \text{at } y = H(x, t), \quad (4.39)$$

while the $O(1)$ contribution from the normal stress balance becomes (at $y = H(x, t)$):

$$\begin{aligned} -P_0 - \frac{2}{Re} H_x u_{0y} + \frac{2}{Re} v_{0y} + \bar{E}_b \left\{ 2H_x \left[\frac{\varepsilon}{2} \tilde{V}_{1y} \right]_{II}^I + \right. \\ \left. \left[\varepsilon \tilde{V}_{1y} \tilde{V}_{2y} \right]_{II}^I - \left[\frac{\varepsilon}{2} \tilde{V}_{1x} \right]_{II}^I \right\} = \frac{\Sigma}{Re} H_{xx}. \end{aligned} \quad (4.40)$$

From the leading order of the kinematic condition (2.30), we obtain

$$v_0 = H_t + u_0 H_x, \quad \text{at } y = H(x, t), \quad (4.41)$$

and the symmetry boundary conditions yield the leading order equations

$$v_0(x, 0, t) = u_{0y}(x, 0, t) = 0. \quad (4.42)$$

Solving (4.36) and using the leading order tangential stress balance (4.39), gives

$$u_0 = C(x, t), \quad (4.43)$$

with the function $C(x, t)$ to be found. The leading order solution v_0 can be found by substituting (4.43) into the continuity equation (4.38), and integrating with respect to y to obtain

$$v_{0y} = -u_{0x} = -C_x \quad \Rightarrow \quad v_0 = -yC_x + C_1(x, t),$$

with $C_1(x, t)$ to be determined. The symmetry condition (4.42) gives $C_1 \equiv 0$ and so

$$v_0 = -yC_x. \quad (4.44)$$

The leading order vertical momentum equation (4.37) is integrated next and use is made of the solution (4.44) to obtain

$$P_0 + \Phi_0 = -\frac{C_x}{Re} + D(x, t). \quad (4.45)$$

The leading order contribution to the van der Waals forces is given by

$$\Phi_0 = \frac{K}{8(H(x, t))^3}. \quad (4.46)$$

The leading order normal stress balance condition (4.40) can now be used to obtain an equation connecting the functions $C(x, t)$ and $D(x, t)$ in terms of H . This is achieved by substituting into (4.40) the u_0 from (4.43), v_0 from (4.44), \tilde{V}_1^I and \tilde{V}_1^{II} from (4.30) and (4.31) gives

$$-P_0 - \frac{2}{Re}C_x + \frac{1}{4}\epsilon_0(1 - \epsilon_p)^2\mathcal{H}(H_x) = \frac{\Sigma}{Re}H_{xx}, \quad (4.47)$$

where the only contribution from the electric field at this order comes from the last terms on the left hand side of (4.2). Substituting P_0 from (4.45) (and using (4.46) also), into (4.47), yields

$$D(x, t) = \Phi_0 - \frac{C_x}{Re} + \bar{E}_b \frac{\epsilon_0}{4}(1 - \epsilon_p)^2\mathcal{H}(H_x) - \frac{\Sigma}{Re}H_{xx}. \quad (4.48)$$

One evolution equation arises from the leading order kinematic condition (4.41) when the solutions (4.43) and (4.44) are substituted and the equation is evaluated at $y = H(x, t)$. Physically, this condition is the leading order mass balance relation and reads

$$H_t + (CH)_x = 0.$$

To obtain a second equation, we consider the x -momentum Navier-Stokes equation at the next order, $O(1)$. This is

$$u_{0t} + u_0 u_{0x} + v_0 u_{0y} = -(P_0 + \Phi_0)_x + \frac{1}{Re}(u_{0xx} + u_{2yy}), \quad (4.49)$$

which implies that

$$u_{2yy} = Re \left(C_t + CC_x - \frac{C_{xx}}{Re} + D_x \right) - C_{xx}. \quad (4.50)$$

Integrating once with respect to y and applying the $O(\varepsilon^2)$ symmetry condition $u_{2y}(x, 0, t) = 0$, yields

$$u_{2y} = yRe \{ C_t + CC_x + D_x \} - 2yC_{xx}. \quad (4.51)$$

The tangential stress balance condition at $O(\varepsilon^2)$ provides the second evolution equation connecting $H(x, t)$ and $C(x, t)$, and is

$$u_{2y} + v_{0x} - u_{0y}H_x^2 - 4u_{0x}H_x = 0 \quad \text{at } y = H(x, t). \quad (4.52)$$

Eliminating $D(x, t)$ from (4.51) by use of (4.48) and substituting the result into (4.52) gives the evolution equation

$$\frac{4(C_x H)_x}{H Re} = C_t + CC_x + \Phi_{0x} + \bar{E}_b \frac{\epsilon_o}{4} (1 - \epsilon_p)^2 \mathcal{H}(H_{xx}) - \frac{\Sigma}{Re} H_{xxx}.$$

The evolution equations

To summarize, the evolution equations to be addressed are

$$H_t + (CH)_x = 0, \quad (4.53)$$

$$C_t + CC_x = \frac{4}{Re} \frac{(HC_x)_x}{H} - \Phi_{0x} - \frac{\epsilon_0}{4} \bar{E}_b (1 - \epsilon_p)^2 + \frac{\Sigma}{Re} H_{xxx}, \quad (4.54)$$

where

$$\Phi_0 = \frac{K}{8(H(x, t))^3}. \quad (4.55)$$

In addition, boundary and initial conditions must also be specified. In the numerical work that follows we adopt periodic boundary conditions which are well-suited for accurate pseudo-spectral calculations.

4.2 Linear Stability Analysis of the Evolution Equations

It is informative to analyze the linear stability of the steady state solution $(C, H) = (0, 1)$ of the evolution equations (4.53) and (4.54). Writing $C = C'$ and $H = 1 + H'$ where primes denote infinitesimally small quantities, substituting into (4.53) and (4.54) and linearizing (note that the linearization of the van der Waals term is $\Phi'_{0x} = -\frac{3K}{8} H'_x$), gives the following linear system

$$H'_t + C'_x = 0, \quad (4.56)$$

$$\frac{4C'_{xx}}{Re} = C'_t - \frac{3}{8} K H'_x + \bar{E}_b \frac{\epsilon_o}{4} (1 - \epsilon_p)^2 \mathcal{H}(H'_{xx}) - \frac{\Sigma}{Re} H'_{xxx}. \quad (4.57)$$

Looking for normal mode solutions in the form $(C', H') = (C_o, H_o)e^{ikx + \omega t}$, where C_o and H_o are constants, a dispersion relation follows in a direct way by insisting on the determinant linear homogeneous system involving C_o and H_o to be zero, in order to guarantee non-trivial solutions. The dispersion relation is:

$$\omega^2 + 4 \frac{k^2}{Re} \omega - \frac{3}{8} k^2 K + \bar{E}_b \frac{\epsilon_o}{4} (1 - \epsilon_p)^2 k^3 \text{sgn}(k) + \frac{\Sigma}{Re} k^4 = 0. \quad (4.58)$$

If we let $\bar{\bar{E}}_b = 0$ and $W_f = \frac{\Sigma}{Re}$, then (4.58) is the same as the long wave dispersion relation found earlier and starting from the full problem.

The general solution of the dispersion relation (4.58) is

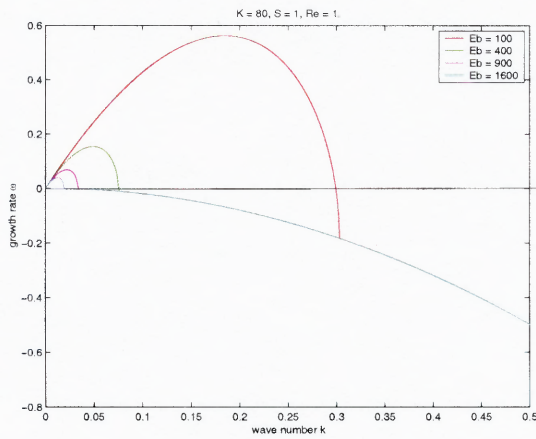
$$\omega = \frac{-\frac{4k^2}{Re} \pm \sqrt{\frac{16k^4}{Re^2} - 4 \left[-\frac{3}{8}k^2K + k^4W_f + k^3 \text{sgn}(k)\bar{\bar{E}}_b \right]}}{2} \quad (4.59)$$

where $\bar{\bar{E}}_b = \bar{E}_b \frac{\epsilon_0}{4} (1 - \epsilon_p)^2$. We see that the solution with the positive sign for the square root can give rise to instability, while the other root is always stabilizing. In what follows we consider the unstable modes alone. The expression for ω shows that for k positive, then both surface tension (which appears through the parameter W_f), and the electric field (appearing through the parameter $\bar{\bar{E}}_b$), stabilize the flow, as opposed to van der Waals forces which are destabilizing. This observation opens the possibility of obtaining enhanced stabilization (in the linear regime) for large enough values of $\bar{\bar{E}}_b$, as we demonstrate next.

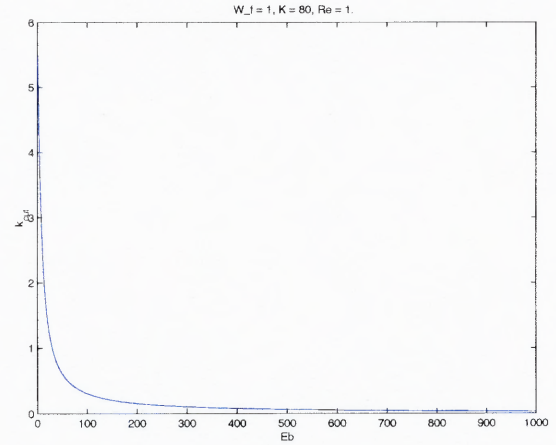
A typical set of results calculated using the dispersion relation (4.59) is given in Figures 4.2(a,b). In both Figures the parameters used are $W_f = Re = 1$ and $K = 80$. Figure 4.2(a) shows the dependence of the growth rate ω on the wavenumber k for a range of $\bar{\bar{E}}_b$ starting at 100 and going to 1600. It can be seen that both the maximum growth rate as well as the band of unstable modes are decreasing as the electric field intensity is increased (i.e. $\bar{\bar{E}}_b$ is increased). In addition, at a value of $\bar{\bar{E}}_b = 1600$ the flow is found to be almost completely stable. This enhanced stabilization can be quantified by considering the critical wavenumber, k_c say, below which the flow is stable. Inspection of the term under the radical in equation (4.59), indicates that if the term in the square bracket is greater than zero, then the real part of ω is negative for all k and so a complete stabilization follows. The value of k_c is found by setting $-\frac{3}{8}k^2K + k^4W_f + k^3\bar{\bar{E}}_b = 0$, which gives

$$k_c = \frac{-\bar{\bar{E}}_b + \sqrt{\bar{\bar{E}}_b^2 + \frac{3}{2}W_fK}}{2W_f}. \quad (4.60)$$

The expression (4.60) shows immediately that in the absence of an electric field, the band of unstable modes has size $(3K/8W_f)^{\frac{1}{2}}$ and so the flow becomes unstable to shorter wavelengths as K is increased and/or W_f is decreased, as would be expected on physical grounds. What is more interesting, however, is the stabilization provided by the electric field. As $\bar{\bar{E}}_b$ increases the critical wavenumber decreases and the behavior for large $\bar{\bar{E}}_b$ is $k_c \sim (3K/8\bar{\bar{E}}_b)$. This behavior is shown clearly in Figure 4.2(b) which shows the variation of k_c with $\bar{\bar{E}}_b$.



(a)



(b)

Figure 4.2 The relation. For (a) wave number k and growth rate ω with different $\bar{\bar{E}}_b$. For (b) $\bar{\bar{E}}_b$ and k_c

CHAPTER 5

NUMERICAL SOLUTION OF THE EVOLUTION EQUATIONS

5.1 Numerical Solutions

In this Chapter, we address the problem numerically. In the numerical work that follows we consider (4.53)-(4.54) and write W_f instead of \bar{E}_b and $u(x, t)$ instead of $C(x, t)$. Inclusion of the van der Waals term from (4.55), gives the following system:

$$H_t + (Hu)_x = 0, \quad (5.1)$$

$$u_t + uu_x = \frac{4}{HRe}(Hu_x)_x - \left(\frac{K}{8H^3}\right)_x - W_e \mathcal{H}(H_{xx}) + W_f H_{xxx}. \quad (5.2)$$

The equations are solved on 2π -periodic domains and the initial conditions are taken to be of the form

$$H(x, 0) = 1 + a_1 \cos(x), \quad u(x, 0) = a_2 \sin(x). \quad (5.3)$$

The parameters a_1 and a_2 are initial amplitudes and the geometry of the problem necessitates $0 < a_1 < 1$. The symmetry of the initial conditions is preserved by the evolution equations and this choice has been made in order to have some prior knowledge regarding the place of singularity formation (sheet rupture), for example. Some additional accuracy checks for the numerical work come from integration of (5.1) and (5.2) over one period; using the class of initial conditions (5.3), we obtain the following conserved quantities

$$\int_0^{2\pi} H(x, t) dt = 0, \quad \int_0^{2\pi} u(x, t) dt = 0. \quad (5.4)$$

The numerical solutions presented here are carried out using pseudo-spectral methods in space and a four-stage Runge-Kutta in time. The time step is adaptive and depends on the number of spatial modes whose amplitudes are greater than some prescribed tolerance, typically between 10^{-9} and 10^{-12} . Further, the solution

is spectrally interpolated when $N/2 - 5$ modes have an amplitude larger than this prescribed criterion, where N is the number of collocation points. The accuracy requirement can be quite severe due to dispersive terms in the dispersion relation, even though all sufficiently large wavenumbers are damped by the viscous terms. This is especially felt at large values of W_f and one way to see this is to drop the viscous term (i.e. formally set $Re = \infty$). Then, the dispersion relation for large wavenumbers k provides solutions proportional to $\exp(ikx \pm ik^2W_f^{1/2}t)$ irrespective of the value of $W_e = O(1)$. These solutions rotate the Fourier modes in the complex plane and to control such rotations we require $k^2\Delta t < \nu$, where ν is sufficiently small and is between 0.1 and 0.8 in our calculations. The code maintains this accuracy restriction.

5.2 The Case of Zero Electric Field and Similarity Solutions

As an accuracy test and an evaluation of the code, we consider the case of zero electric field, $W_e = 0$. This problem has been solved numerically by Vaynblat, Lister and Witelski [19], and we reproduce their results first before adding the effects of the electric field into the nonlinear evolution. In the calculations of [19], the periodic domain is taken to be $[-1, 1]$ and their equivalent of our equation (5.2) is

$$u_t + uu_x = \frac{4}{H}(Hu_x)_x - (H^{-3})_x + 3Sh_{xxx},$$

where S is their surface tension parameter. Our 2π -periodic domains, and different non-dimensionalization, make it necessary to take the following parameter values in order to make a direct comparison

$$Re = \frac{1}{\pi}, \quad K = 8, \quad W_f = \frac{3}{2}.$$

In addition, the appropriate initial conditions for these comparisons are

$$H(x, 0) = 1 + 0.2 \cos(x), \quad u(x, 0) = -0.1 \sin(x). \quad (5.5)$$

Figures 5.1(a,b) show the evolution of the interface and the corresponding horizontal velocity in the absence of an electric field ($W_e = 0$) and for the parameters given above. Our results reproduce accurately the calculations in [19]. The time to rupture according to our results is $t_r = 4.78437956$ and dividing this by π due to the difference in time scales between our simulations and those in [19], we get $t_* \sim 1.5229\dots$ in complete agreement with that paper (See Section IIIA of [19]). Figures 5.2(a-c) show the evolution of the minimum film thickness, H_{min} , the maximum horizontal velocity, u_{max} , and the maximum derivative of the horizontal velocity, $\max(u_x)$, where it is understood that maxima or minima are taken over the domain $[0, 2\pi)$. The Figures display very clearly the sudden appearance of the singularity and the short time scale over which it drives the film to pinching. This is typical in van der Waals driven rupture and has been documented by different authors (see Introduction).

The original numerical study of the zero electric field problem by Ida and Miksis [8], suggested the formation of similarity solutions of the second type near rupture. The computations of Vaynblat et al. [19], however, were able to resolve the fast dynamics near pinching using adaptive gridding techniques, and give strong support to similarity solutions of the first kind with the dominant balances being between inertia, viscosity and van der Waals forces, with surface tension forces being negligible near rupture. It has been suggested, and is confirmed numerically, that the following similarity solutions hold near the singular time t_r and rupture point $x = x_r$,

$$H(x, t) = \tau^\alpha F(\eta), \quad u(x, t) = \tau^\gamma G(\eta), \quad \eta = \frac{x - x_r}{\tau^\beta}, \quad (5.6)$$

where $\tau = t_r - t$ and the constants α , β , and γ are scaling exponents to be determined. We note that the Ida and Miksis [8] similarity solutions balance van der Waals forces with viscosity while inertia and surface tension are both subdominant, and this gives $\alpha = 1/3$ with β left undetermined. Balancing all terms besides surface tension,

however, determines all exponents, and these are given by

$$\alpha = \frac{1}{3}, \quad \beta = \frac{1}{2}, \quad \gamma = -\frac{1}{2}. \quad (5.7)$$

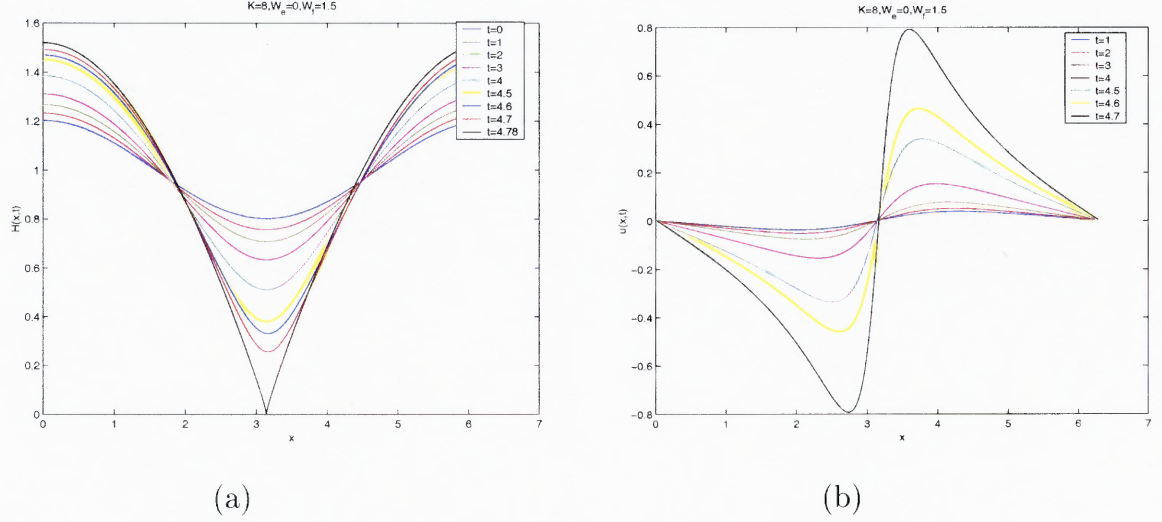


Figure 5.1 The evolution of $H(x,t)$ and $u(x,t)$ for $Re = 1/\pi$, $K = 8$, $W_e = 0$, $W_f = 1.5$. (a) The evolution of $H(x,t)$. (b) The evolution of $u(x,t)$.

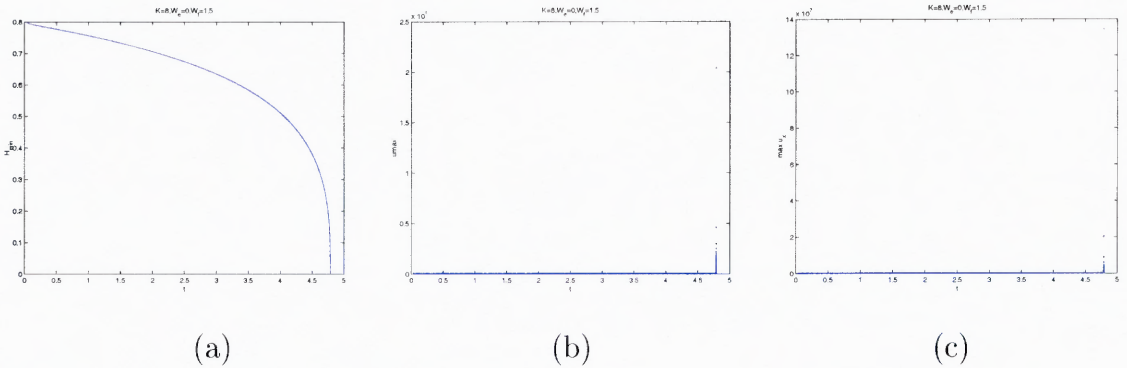


Figure 5.2 No electric field. Evolution of (a) H_{min} , (b) u_{max} and (c) $\max(u_x)$ for $K = 8$, $W_e = 0$, $W_f = 1.5$.

The scaling exponents (5.7) and the similarity solutions (5.6), can be confirmed numerically by plotting appropriate variables on log-log scales. Such plots have been given by Vaynblat et al. [19], and we generate equivalent ones here in order to provide a basis for our non-zero electric field computations. This can be done

Table 5.1 Estimation of scaling exponents for no electric field

Quantity	Theoretical	Computed
u_x	$\frac{\gamma-\beta}{\alpha} = -3$	-2.953
$-H_t$	$\frac{\alpha-1}{\alpha} = -2$	-1.951
H_{xx}	$\frac{\alpha-2\beta}{\alpha} = -2$	-1.634
$\max(u)$	$\frac{\gamma}{\alpha} = -1.5$	-1.673
$\max(H_x)$	$\frac{\alpha-\beta}{\alpha} = -0.5$	-0.220

by plotting different variables against the minimum film thickness. Regression can then be used to estimate slopes. Following [19], we consider the following variables: $u_x(\pi, t)$, $-H_t(\pi, t)$, $H_{xx}(\pi, t)$, $u_{\max}(t)$, $\max(H_x)$. For example, regression on u_x should give us an estimate for $(\gamma - \beta)/\alpha$, regression on $-H_t$ an estimate for $(\alpha - 1)/\alpha$, etc. Table 5.1 shows the results of the regression of the data taken from the runs of Figures 5.1(a) and (b), along with the theoretically predicted values according to (5.7).

5.3 Non-zero Electric Field

We consider next the inclusion of the electric field into the nonlinear evolution. We note, first, that the similarity solutions and scales (5.6) and (5.7) are still consistent structures as a singularity forms. To see this, we can use these solutions to estimate the size of the electric field term compared to the terms retained, and find that it is asymptotically smaller; this must be so, since the electric field effects are asymptotically smaller than surface tension forces as rupture develops, and the latter are excluded from the main balances also.

We begin, therefore, with a typical situation and aim to confirm numerically the similarity solutions described above. This run has $Re = 1/\pi$, $K = 8$, $W_f = 1.5$ and $W_e = 0.5$. We begin with the evolution of $H(x, t)$ and $u(x, t)$ given in Figures

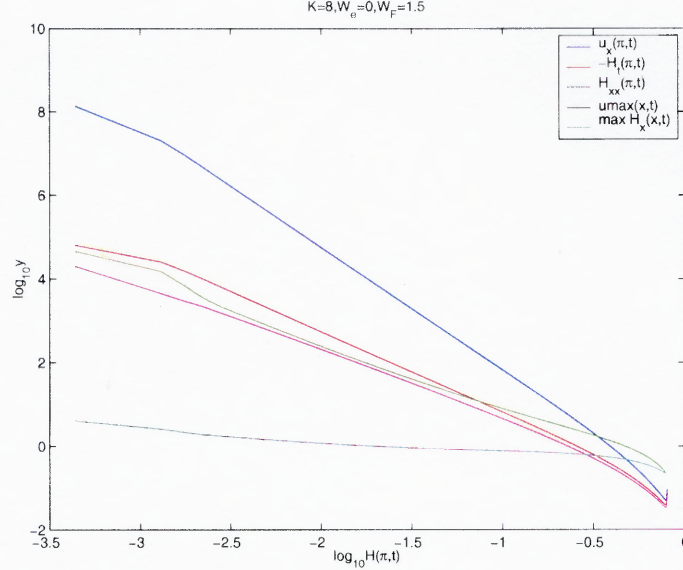


Figure 5.3 The relation between $\log_{10}H(\pi, t)$ with $u_x(\pi, t)$, $-H_t(\pi, t)$, $H_{xx}(\pi, t)$, $umax(x, t)$, and $\max(H_x(x, t))$ respectively. Computed slopes are given in Table 5.1.

5.4(a-b). We see that rupture still takes place, but the main effect of the electric field is to delay this event. The time of rupture is about $t_r = 5.611$ in this case, compared to approximately 4.784 in the absence of an electric field. The initial conditions are the same as before, namely equation (5.3). In the accompanying Figures 5.5(a-c) we show the corresponding evolution of H_{min} , $max(u)$ and $max(u_x)$, and the behavior is qualitatively similar to the zero electric field case. In Figure 5.6 we present log-log plots of various quantities (see earlier description) in the aim of extracting the scaling exponents by regression. The behavior is qualitatively similar to the zero electric field case, and in Table 5.2 we present the regression results.

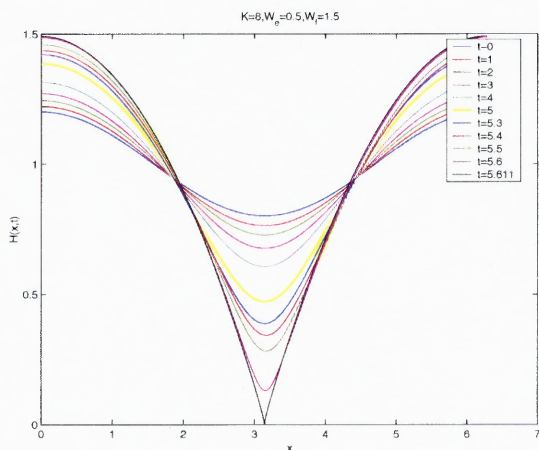
Another measure of the singularity formation is available from the energy-norms of the solution defined as

$$E(t) = \int_0^{2\pi} (H^2 + u^2) dx.$$

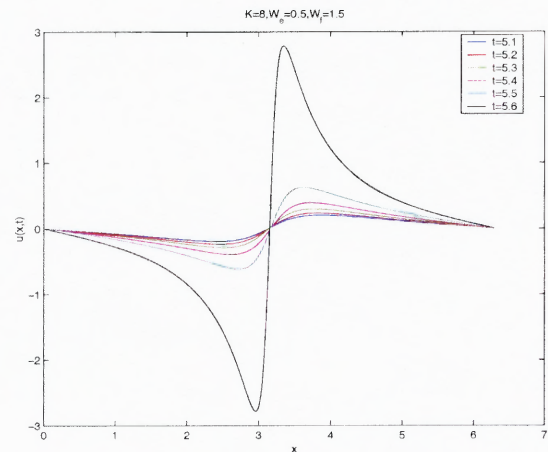
A comparison of this quantity in the absence and presence of the electric field, and in particular for the values $K = 8$, $W_f = 1.5$ and $W_e = 0$ and 0.5 respectively, see

Table 5.2 Estimation of scaling exponents in the presence of an electric field

Quantity	Theoretical	Computed
u_x	$\frac{\gamma-\beta}{\alpha} = -3$	-2.960
$-H_t$	$\frac{\alpha-1}{\alpha} = -2$	-1.958
H_{xx}	$\frac{\alpha-2\beta}{\alpha} = -2$	-1.820
$\max(u)$	$\frac{\gamma}{\alpha} = -1.5$	-1.703
$\max(H_x)$	$\frac{\alpha-\beta}{\alpha} = -0.5$	-0.213



(a)



(b)

Figure 5.4 Electric field present. $K = 8$, $W_e = 0.5$, $W_f = 1.5$. (a) Evolution of $H(x, t)$, (b) evolution of $u(x, t)$.

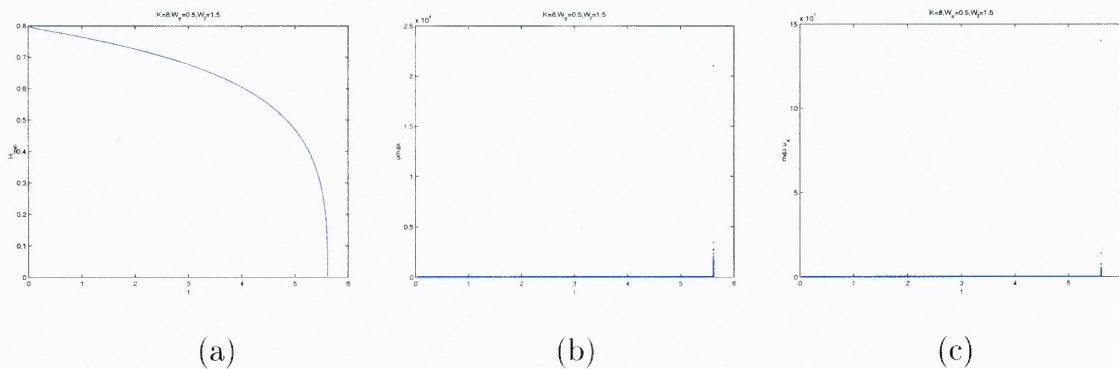


Figure 5.5 Electric field present. $K = 8$, $W_e = 0.5$, $W_f = 1.5$. (a) Evolution of H_{min} . (b) Evolution of $max(u)$. (c) Evolution of $max(u_x)$.

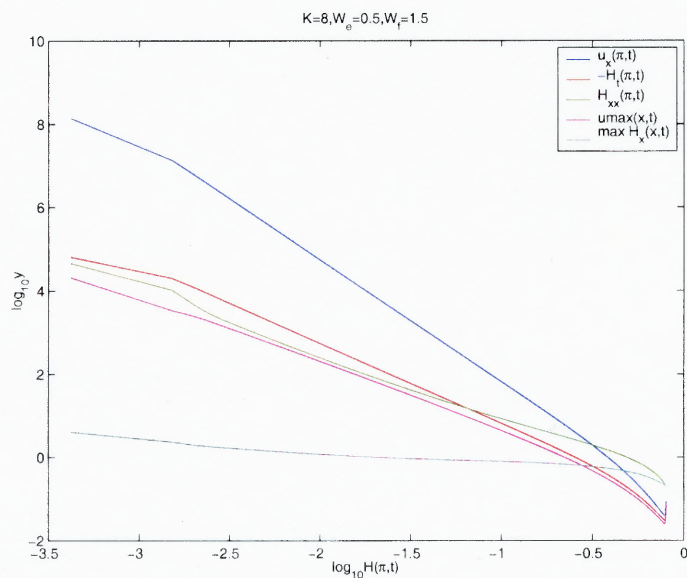


Figure 5.6 The relation between $\log_{10}H(\pi, t)$ with $u_x(\pi, t)$, $-H_t(\pi, t)$, $H_{xx}(\pi, t)$, $umax(x, t)$, and $\max(H_x(x, t))$ respectively. Computed slopes are given in Table 5.2.

Figures 5.7(a-b). It can be seen that $E(t)$ blows up in a finite time as expected (the contributor to this is the u^2 term) and the delay in the singularity due to the stabilizing effect of the electric field is very clear from the Figures.

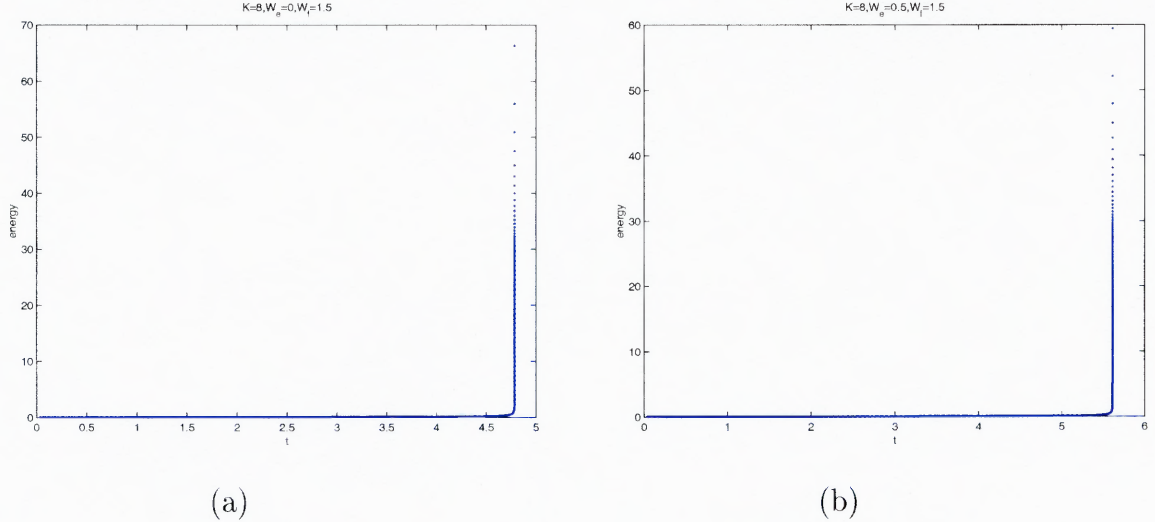


Figure 5.7 Evolution of $E(t) = \int_0^{2\pi} (H^2 + u^2) dx$, $K = 8$, $W_f = 1.5$. (a) No electric field, $W_e = 0$. (b) $W_e = 0.5$.

In Figures 5.8(a-b), we show numerical solutions using the initial conditions (5.3) and a relatively large electric field having $W_e = 2.0$. We note that the initial disturbance is relatively large and is outside the regime covered by linear stability theory. This will become an important observation in the discussion of the results. The Figures show that as t gets large the interface becomes flat and the velocity goes to zero; the film is stabilized and the van der Waals destabilizing forces are overcome by the electric field. Consequently, rupture does not take place. Additional evidence of this stabilization is given in Figures 5.9(a-c) which depict the evolution of H_{min} , $max(u)$ and $max(u_x)$, respectively. The former tends to 1 after about 300 time units while the latter quantities tend to zero, as would be expected. The slow stabilization scale is due to the fact that we are very close to a threshold value above which the film evolves to a uniform state for the initial conditions used here. At values lower than $W_e = 2$, the film evolves to a finite time singularity. We emphasize that the initial

conditions play a crucial role in this conclusion. The results we are describing are in the nonlinear regime and it is expected that the threshold value of approximately $W_e \approx 2$ is a function of the initial conditions, everything else kept the same.

A summary of results regarding rupture for the initial conditions (5.3) and different W_e with $Re = 1/\pi$, $K = 8$, $W_f = 1.5$, is given in Figure 5.10 which shows the variation of the time to rupture, t_r , with the electric capillary number W_e . As mentioned above, the initial conditions play an important role in the dynamics since we are in a regime that is linearly stable (for the periodic problem considered here). This is discussed from a linear stability perspective next. It can be seen from the Figure that the time to rupture increases as the electric field parameter W_e increases, and in fact it recedes to infinity as we approach a value of W_e near 2. For values of $W_e > 2$, we find no rupture and an evolution to a quiescent flat state takes place instead. It has also been confirmed that the time taken to reach this steady state slows down as we approach the critical value of W_e from above. At the same time, it decreases as W_e increases.

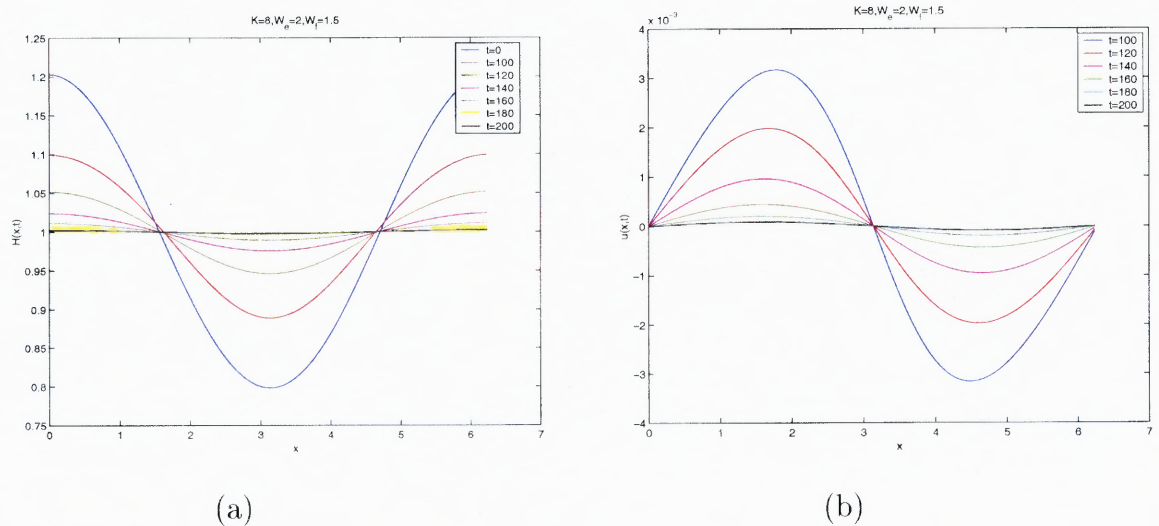


Figure 5.8 Relatively large electric field, $W_e = 2.0$, showing stabilization. (a) Evolution of $H(x,t)$. (b) Evolution of $u(x,t)$.

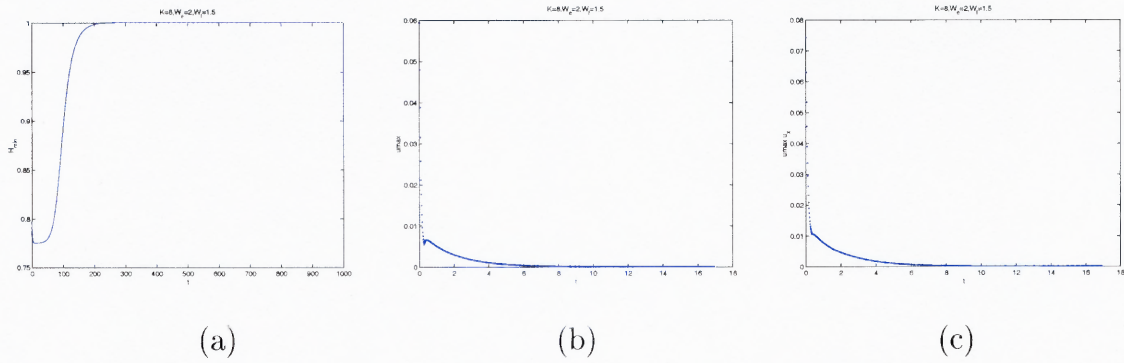


Figure 5.9 Relatively large electric field, $W_e = 2.0$, showing stabilization. $K = 8$, $W_e = 2$, $W_f = 1.5$. (a) Evolution of H_{min} . (b) Evolution of $\max(u)$. (c) Evolution of $\max(u_x)$.

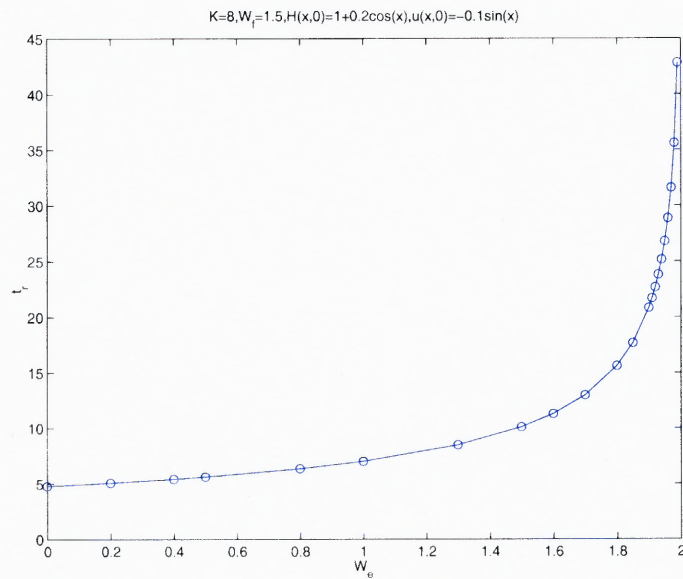


Figure 5.10 Rupture time as a function of W_e for the set of initial conditions (5.3).

We turn next to the issue of complete stabilization found above. It has been shown that a linear stability of the evolution equations (5.1) and (5.2), provides a critical wavenumber above which the flow is linearly stable. This critical wavenumber is given by

$$k_c = \frac{-W_e + \sqrt{W_e^2 + \frac{3}{2}W_f K}}{2W_f}. \quad (5.8)$$

Since we are computing on 2π -periodic domains, the wavenumbers take on integer values and the result (5.8) is derivable through a Fourier series representation of solutions which require integer values for the wavenumber. If the parameters are such that $k_c < 1$, then, then the flow is linearly stable for all waves that we are computing numerically. Taking $K = 8$ and $W_f = 3/2$, it is easy to show that the threshold value of W_e that gives $k_c = 1$, is given by $W_e = 3/2$. As far as our numerical computations are concerned, then, the flow for $W_e > 3/2$ (all other parameters kept as before), is linearly stable. We demonstrate this next by computations of the nonlinear system.

We use the following initial conditions

$$H(x, 0) = 1 + 0.01 \cos(x), \quad u(x, 0) = 0, \quad (5.9)$$

where the perturbation amplitude is 10^{-2} and is considered to be within the linear regime. Two cases are considered. The first above threshold and having $W_e = 1.55$ and the second just below threshold with $W_e = 1.45$. We expect the former solution to be stable and to evolve to a uniform quiescent state, while the latter should rupture at finite time. This is indeed the case as Figures 5.13 and 5.14 show. The Figures show the evolution of $H(x, t)$ and $u(x, t)$ for the two values. The stabilization above threshold is clearly seen in Figure 5.13 with the film becoming flat at large times which are about 2000 time units as seen from the accompanying Figures 5.12(a-c). For $W_e = 1.45$, however, we observe from Figure 5.13(a-b) a long adjustment of

the flow until the weak linear instability has a chance to amplify the flow into the nonlinear regime and rupture. The rupture time is approximately equal to 482.23. Additional support for this is given in Figures 5.14(a-c) for the related quantities H_{min} , $max(u)$ and $max(u_x)$.

Finally, in Figures 5.15 and 5.16, we provide a collection of the results for the small amplitude initial condition. In Figure 5.15 we give the evolution of $H_{min}(t)$ for $K = 8$ and $W_f = 1.5$ for a range of values of the electric field parameter $W_e = 0, 0.5, 1.0$ and 1.5 . With the exception of $W_e = 1.5$ which is at threshold, all other parameters are below the linear stability threshold and rupture is expected. This is confirmed by the results which also shows a stabilization in the sense that the singularity time is delayed.

At larger values of W_e we obtain stabilization with the large time evolution giving a flat quiescent state. Representative results for $W_e = 1.5, 2.0$ and 5.0 are shown in Figure 5.16. It can be observed that as W_e increases the flow adjusts to its uniform steady state in a smaller time.

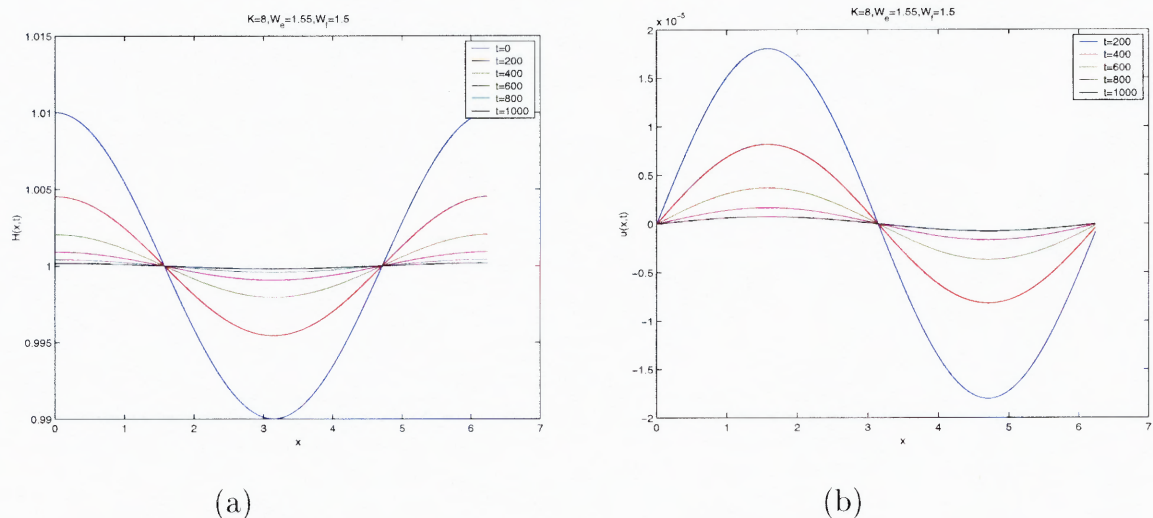


Figure 5.11 Small amplitude initial conditions $H(x,0) = 1 + 0.01 \cos(x)$ and $W_e = 1.55$. (a) The evolution of $H(x,t)$. (b) The evolutions $u(x,t)$.

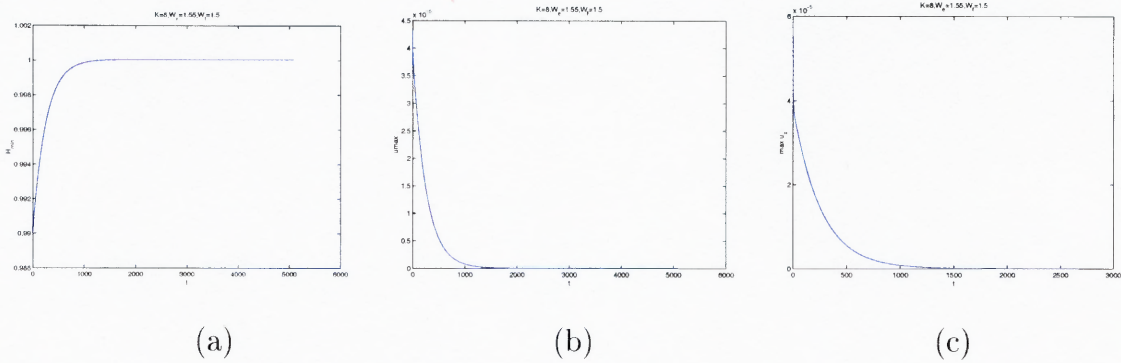


Figure 5.12 Initial conditions $u(x, 0) = 0$, $H(x, 0) = 1 + 0.01 \cos(x)$, $W_e = 1.55$. Behavior above linear threshold. (a) Evolution of H_{min} . (b) Evolution of $\max(u)$. (c) Evolution of $\max(u_x)$.

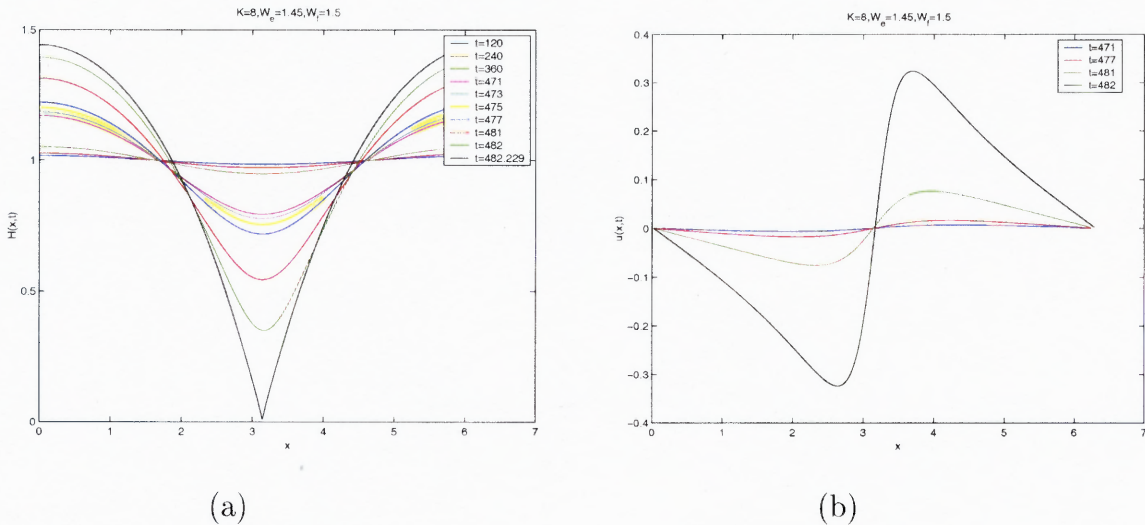


Figure 5.13 Initial conditions $u(x, 0) = 0$, $H(x, 0) = 1 + 0.01 \cos(x)$, $W_e = 1.45$. (a) The evolution of $H(x, t)$. (b) The evolutions $u(x, t)$.

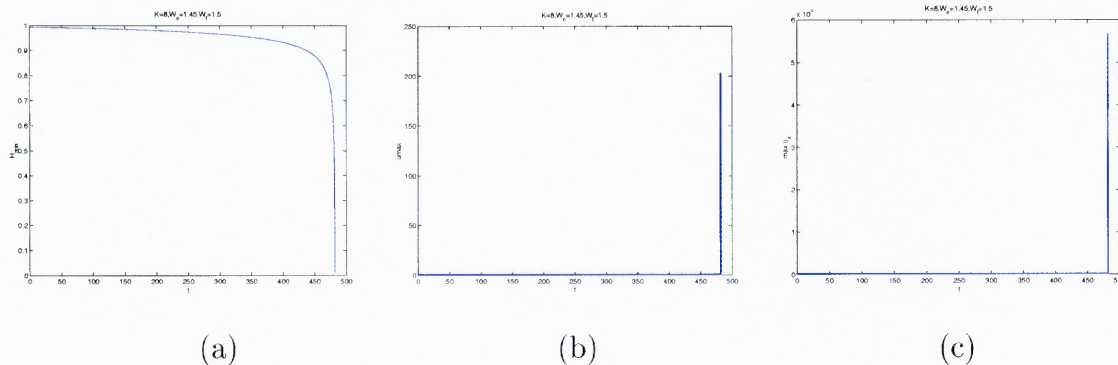


Figure 5.14 Initial conditions $u(x, 0) = 0$, $H(x, 0) = 1 + 0.01 \cos(x)$, $W_e = 1.45$. Behavior below linear threshold. (a) Evolution of H_{min} . (b) Evolution of $max(u)$. (c) Evolution of $max(u_x)$.

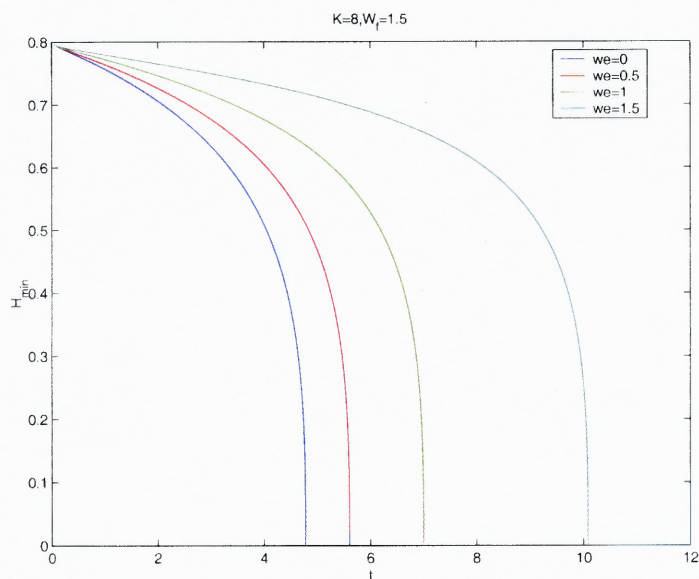


Figure 5.15 Initial conditions $H(x, 0) = 1 + 0.01 \cos(x)$, $u(x, 0) = 0$. $K = 8$, $W_f = 1.5$, $Re = 1/\pi$. Evolution of H_{min} for increasing values of W_e .

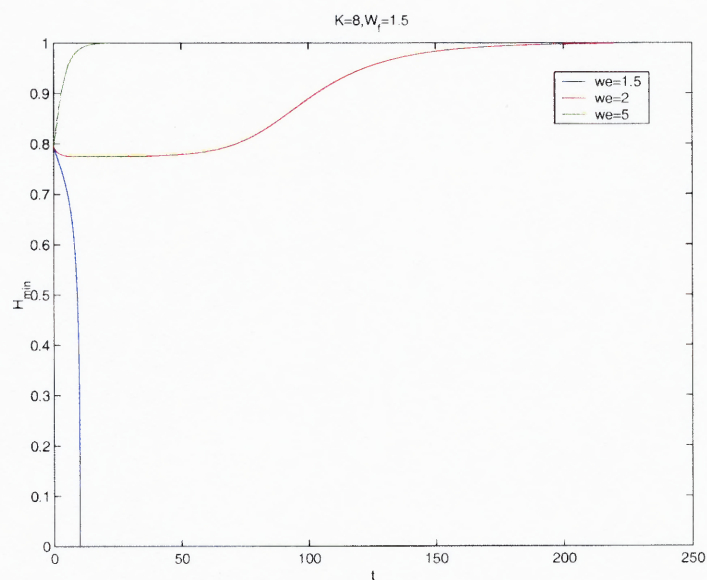


Figure 5.16 Initial conditions $H(x, 0) = 1 + 0.01 \cos(x)$, $u(x, 0) = 0$. $K = 8$, $W_f = 1.5$, $Re = 1/\pi$. Evolution of H_{min} for increasing values of W_e .

CHAPTER 6

CONCLUSIONS

In the present work, we examined the effect of an axial electric field on the rupture dynamics of a thin viscous liquid film subject to attractive van der Waals molecular forces. The liquid was assumed to be non-conducting electrically. This was undertaken in order to determine whether the electric field can be used as an additional control parameter in applications where rupture of the thin liquid film is an undesirable outcome.

Our study began with the two-dimensional Navier-Stokes equations for the fluid motion coupled to Laplace equations for the electric field potentials. The two physical problems are coupled through polarization forces that develop at the interface between the liquid and the surrounding passive medium. A linear stability analysis of the resulting set of equations was performed. We determined that one can always choose a value of the electric field magnitude (through the electric capillary number) so that a linearly unstable flow (due to the attractive van der Waals force) is stabilized. Also, a long-wave asymptotic analysis of the full set of equations was performed in order to determine the nonlinear stability properties of perturbations of the (flat) basic state of the flow. A pseudo-spectral solver was employed to numerically simulate rupturing films and determine the effect of the electric field on the dynamics of the process. Significantly, we found that the rupturing solution in the presence of an electric field exhibits similarity of the first-kind which is delayed relative to the case of rupture in the absence of electric forces. Further, we determined and verified the presence of an electric field amplitude past which the van der Waals unstable flow is completely regularized in the long-wave regime.

BIBLIOGRAPHY

- [1] J. BURELBACH, G. BANKOFF, AND S. DAVIS, *Nonlinear stability of evaporating/condensing liquid films*, J. Fluid Mech., 195 (1988).
- [2] B. DERYAGIN, *The definition and magnitude of disjoining pressure and its role in statics and dynamics of thin films*, Colloid Journal USSR, 17 (1955), p. 207.
- [3] M. F. EL-SAYED, *Electro-aerodynamic instability of thin dielectric liquid sheet sprayed with an air stream*, Phys. Rev.E 60, 60 (1999).
- [4] T. ERNEUX AND S. H. DAVIS, *Nonlinear rupture of free films*, Phys. Fluid A, 5 (1993), p. 1117.
- [5] T. ERNEUX, E. L. REISS, J. F. MAGNAN, AND P. K. JAYAKUMAR, *Nonlinear stability control and λ -bifurcation*, SIAM Journal on Applied Mathematics, 47 (1987).
- [6] A. GONZALEZ AND A. CASTELLANOS, *Nonlinear electrohydrodynamic waves on films falling down an inclined plane*, Physical Review E, 53(4) (1996).
- [7] R. J. GUMERMAN AND G. M. HOMSEY, *The stability of radially bounded thin films*, Chem. Eng. Commun., 2 (1975), p. 27.
- [8] M. P. IDA AND M. MIKSYS, *Thin film rupture*, Appl. Math. Lett., 9 (1996).
- [9] M. P. IDA AND M. J. MIKSYS, *The dynamics of thin films i: General theory*, SIAM J. Appl. Math., 58 (1998).
- [10] —, *The dynamics of thin films ii: Applications*, SIAM J. Appl. Math., 58 (1998).
- [11] J. R. MELCHER AND J. SCHWARZ, *Interfacial relaxation overstability in a tangential electric field*, Phys. Fluids, 11 (1968).
- [12] A. ORON, S. H. DAVIS, AND S. G. BANKOFF, *Long-scale evolution of thin liquid films*, Reviews of Modern Physics 69, 69 (1997).
- [13] J. T. G. OVERBEEK, *Black soap films*, The Journal of Physical Chemistry, 64 (1960).
- [14] M. PREVOST AND D. GALLETZ, *Nonlinear rupture of thin free liquid films*, J. Chem. Phys., 84 (1986).
- [15] —, *Nonlinear stability of thin free liquid films: rupture and marangoni effects*, AIChE. Symp. Sur., 252 (1986), p. 123.
- [16] E. RUCKENSTEIN AND R. K. JAIN, *Spontaneous of thin liquid films*, J. Chem. Soc. Faraday Trans. II, 70 (1974), p. 132.
- [17] A. SHARMA AND E. RUCKENSTEIN, *Rupture of thin free films with insoluble surfactants: nonlinear aspects*, AIChE. Symp. Sur., 252 (1986), p. 130.

- [18] P. G. TILLEY, B. S. PETROPOULOS AND D. T. PAPAGEORGIU, *Dynamics and rupture of planar electrified liquid sheets*, Phys. Fluids, 13 (2002), p. 3547.
- [19] D. VAYNBLAT, J. R. LISTER, AND T. P. WITELSKI, *Rupture of thin films by van der waals forces: Evolution and self-similarity*, Phys. Fluids, 13 (2001), p. 1130.
- [20] A. VRIJ, *Possible mechanism for the spontaneous rupture for thin free liquid films*, Discuss. Faraday Soc., 42 (1996), p. 23.
- [21] H. WENDEL, D. GALLEZ, AND P. BISCH, *On the dynamic stability of fluid dielectric films*, Journal of Colloid and Interface Science, 84(1) (1981).
- [22] M. B. WILLIAMS AND S. H. DAVIS, *Nonlinear theory of thin film rupture*, J. Colloid Interface Sci., 90 (1982), p. 220.
- [23] T. P. WITELSKI AND A. J. BERNOFF, *Stability of self-similarity solutions for van der waals driven thin film rupture*, Physics of fluids, 11 (1999).
- [24] W. W. ZHANG AND J. R. LISTER, *Similarity solutions for van der waals rupture of a thin film*, Physics of fluids, 11 (1999).